UPPSALA
UNIVERSITET

Digital Comprehensive Summaries of Uppsala Dissertations from the Faculty of Science and Technology 1298

A study of the structure and dynamics of Saturn's inner plasma disk

MIKA HOLMBERG

ACTA
UNIVERSITATIS
UPSALIENSIS
UPPSALA
2015

ISSN 1651-6214
ISBN 978-91-554-9353-0
urn:nbn:se:uu:diva-263278

Dissertation presented at Uppsala University to be publicly examined in Lägerhyddsvägen 1, Uppsala, Thursday, 19 November 2015 at 13:00 for the degree of Doctor of Philosophy. The examination will be conducted in English. Faculty examiner: Professor Thomas Cravens (University of Kansas).

Abstract
Holmberg, M. 2015. A study of the structure and dynamics of Saturn's inner plasma disk. *Digital Comprehensive Summaries of Uppsala Dissertations from the Faculty of Science and Technology* 1298. 53 pp. Uppsala: Acta Universitatis Upsaliensis. ISBN 978-91-554-9353-0.

This thesis presents a study of the inner plasma disk of Saturn. The results are derived from measurements by the instruments on board the Cassini spacecraft, mainly the Cassini Langmuir probe (LP), which has been in orbit around Saturn since 2004. One of the great discoveries of the Cassini spacecraft is that the Saturnian moon Enceladus, located at 3.95 Saturn radii (1 R_S = 60,268 km), constantly expels water vapor and condensed water from ridges and troughs located in its south polar region. Impact ionization and photoionization of the water molecules, and subsequent transport, creates a plasma disk around the orbit of Enceladus. The plasma disk ion components are mainly hydrogen ions H^+ and water group ions W^+ (O^+, OH^+, H_2O^+, and H_3O^+). The Cassini LP is used to measure the properties of the plasma. A new method to derive ion density and ion velocity from Langmuir probe measurements has been developed. The estimated LP statistics are used to derive the extension of the plasma disk, which show plasma densities above ~20 cm^{-3} in between 2.7 and 8.8 R_S. The densities also show a very variable plasma disk, varying with one order of magnitude at the inner part of the disk. We show that the density variation could partly be explained by a dayside/nightside asymmetry in both equatorial ion densities and azimuthal ion velocities. The asymmetry is suggested to be due to the particle orbits being shifted towards the Sun that in turn would cause the whole plasma disk to be shifted. We also investigate the ion loss processes of the inner plasma disk and conclude that loss by transport dominates loss by recombination in the entire region. However, loss by recombination is still important in the region closest to Enceladus (~±0.5 R_S) where it differs with only a factor of two from ion transport loss.

Keywords: Planetary magnetospheres, Saturn, magnetospheric dynamics, Saturn's inner plasma disk, ring plasma, ion densities, ion velocities, dayside/nightside asymmetry, ion loss rates, Cassini, Langmuir probe, RPWS

Mika Holmberg, Swedish Institute of Space Physics, Uppsala Division, Box 537, Uppsala University, SE-75121 Uppsala, Sweden. Department of Physics and Astronomy, Space Plasma Physics, 516, Uppsala University, SE-751 20 Uppsala, Sweden.

ISSN 1651-6214
ISBN 978-91-554-9353-0
urn:nbn:se:uu:diva-263278 (http://urn.kb.se/resolve?urn=urn:nbn:se:uu:diva-263278)

"In science one tries to tell people,
in such a way as to be understood by everyone,
something that no one ever knew before.
But in the case of poetry, it's the exact opposite!"
- Paul Dirac

List of papers

This thesis is based on the following papers, which are referred to in the text by their Roman numerals.

I *Ion densities and velocities in the inner plasma torus of Saturn*
M. K. G. Holmberg, J.-E. Wahlund, M. W. Morooka, A. M. Persoon
Planetary and Space Science 73, 151-160, 2012

II *Dayside/nightside asymmetry of ion densities and velocities in Saturn's inner magnetosphere*
M. K. G. Holmberg, J.-E. Wahlund, M. W. Morooka
Geophysical Research Letters 41, 3717-3723, 2014

III *Transport and chemical loss rates in Saturn's inner plasma disk*
M. K. G. Holmberg, J.-E. Wahlund, E. Vigren, F. Bagenal, T. A. Cassidy, D. J. Andrews
Submitted

IV *Density structures, ion drift speeds, and dynamics in Saturn's inner plasma disk*
M. K. G. Holmberg, O. Shebanits, J.-E. Wahlund
To be submitted

List of papers not included in the thesis

V *Dusty plasma in the vicinity of Enceladus*
M. W. Morooka, J.-E. Wahlund, A. I. Eriksson, W. M. Farrell, D. A. Gurnett, W. S. Kurth, A. M. Persoon, M. Shafiq, M. André, **M. K. G. Holmberg**
Journal of Geophysical Research 116, A12221, 2011

VI *The detection of energetic electrons with the Cassini Langmuir probe at Saturn*
P. Garnier, J.-E. Wahlund, **M. K. G. Holmberg**, M. W. Morooka, S. Grimald, A. Eriksson, P. Schippers, D. A. Gurnett, S. M. Krimigis, N. Krupp, A. Coates, F. Crary, G. Gustafsson
Journal of Geophysical Research 117, A10202, 2012

VII *Energetic electron observations of Rhea's magnetospheric interaction*
E. Roussos, P. Kollmann, N. Krupp, C. Paranicas, S. M. Krimigis, D. G. Mitchell, A. M. Persoon, D. A. Gurnett, W. S. Kurth, H. Kriegel, S. Simon, K. K. Khurana, G. H. Jones, J.-E. Wahlund, **M. K. G. Holmberg**
Icarus 221(1), 116-134, 2012

VIII *Dust-plasma interaction through magnetosphere-ionosphere coupling in Saturn's plasma disk*
S. Sakai, S. Watanabe, M. W. Morooka, **M. K. G. Holmberg**, J.-E. Wahlund, D. A. Gurnett, W. S. Kurth
Planetary and Space Science 75, 11-16, 2013

IX *The influence of the secondary electrons induced by energetic electrons impacting the Cassini Langmuir probe at Saturn*
P. Garnier, **M. K. G. Holmberg**, J.-E. Wahlund, G. R. Lewis, S. R. Grimald, M. F. Thomsen, D. A. Gurnett, A. J. Coates, F. J. Crary, I. Dandouras
Journal of Geophysical Research Space Physics 118, 7054-7073, 2013

X *Deriving the characteristics of warm electrons (100-500 eV) in the magnetosphere of Saturn with the Cassini Langmuir probe*
P. Garnier, **M. K. G. Holmberg**, J.-E. Wahlund, G. R. Lewis, P. Schippers, A. J. Coates, D. A. Gurnett, J. H. Waite, I. Dandouras
Planetary and Space Science 104, 173-184, 2014

XI *Effects of Saturn's magnetospheric dynamics on Titan's ionosphere*
N. J. T. Edberg, D. J. Andrews, C. Bertucci, D. A. Gurnett, **M. K. G. Holmberg**, C. M Jackman, W. S. Kurth, J. D. Menietti, H. J. Opgenoorth, O. Shebanits, E. Vigren, J.-E. Wahlund
Accepted

Contents

Acknowledgement

First and foremost I'd like to thank my supervisor Jan-Erik Wahlund, who always took time to discuss with me whenever I knocked on his door; something that I truly appreciate and are very thankful for. I'm very grateful for his guidance, enthusiasm for my work, and especially for letting me do things my way, which sometimes included going to the other side of the planet. A great thanks to my unofficial supervisor Michiko Morooka who taught me a lot about Langmuir probe data analysis, being a researcher, and who let me follow her on work trips around the world, both to Japan and to the USA. あたたか いご指導に、心より感謝いたします。Thanks to my assistant supervisors Nikolai Piskunov, for teaching me about accretion disks, and Svetlana Ratynskaia, for asking the hard questions. I'm grateful to Professor Mats André for welcoming me to IRF and for his almost endless patience. Thanks to Anders Eriksson for letting me disturb you with my never ending stream of questions and for trusting me to teach the Space Physics course. Which for me as a student was the most inspiring course at Uppsala University. A huge thank you to all my fellow PhD students: Cecilia (an important member of the night shift gang), Oleg (best kohai ever), Ilka, Elin, Andreas, Elias, Karin, and Erik, and post-docs: David, Daniel (the supreme secretary of the night shift gang), Niklas, Ulrich, Shiyong, Huishan, Laurianne, Hugo, Sergio, Erik, and Megan, that made my stay at the IRF full of joy by apart from work also include crosswords, board games, beers, cinema, slack lining, ping-pong, and a lot of laughs. I would also like to thank the rest of the night shift gang: Thomas, Fredrik, and Reine. And, of course, also all my other co-workers at IRF.

I also want to thank the people on the other side of the planet. Thanks to Professor Obara, Takanori-san, Septi-san, and all the other amazing people at Tohoku University. I would like to thank Krishan Khurana, Margaret Kivelson, and Katherine Ramer for welcoming me to UCLA during my short stay there. And a big thank you to Fran Bagenal, Rob Wilson, and Frank Crary for welcoming me to LASP during my stay there.

I am very grateful for the funding that has made this research possible, to the Swedish Institute of Space Physics, the Royal Swedish Academy of Sciences, Zonta International, Uppsala University, and especially to the Swedish National Space Board.

A huge thank you to all of my amazing family for the loving support throughout the years. To my first family: mamma, pappa, Bea, Sanna, Matt, Michael, Kristoffer, Inger, Göran, Cecilia, Samuel, Marc, Aurora, Ellinor, Torgny, Caela, Jemma, Aveline, and especially mormor Elsa Holmberg: Du är världens bästa mormor! And to Ingemar and Hildur: Jag saknar er. To my second family, my flatmates and dear friends Peter, Anna, Johan, and Sofia. You are the best second family one could ever wish for! And to my extended family Johan L (I'm so flattered that you use me as your TP question corrector), Johanna (you always understand), Elin (my dear fellow adventurer), Zelda (you are the

master of pep talks), Ginah (I'm already longing for the next hike), Rosita (the forest is now waiting for us), Bella (for all the laughs and stickers), and to all the lovely members of UPFAK. For their love and support: Tor, Sara, and Andreas. And to the one person who has given me the most support over the last ten years, Johan. I'll be grateful for the rest of my life.

1. Introduction

The night sky has fascinated humans since the beginning of our history, a fascination that only became larger with the invention of the telescope in the 17th century. The Italian scientist Galileo Galilei (1564 – 1642) used the telescope to study Saturn, a planet that has been known and observed since prehistoric time. The investigation resulted in the first recorded observation of Saturn's rings. However, Galileo mistook the rings for two small planets located, at the time of observation, on each side of the planet. At later observations the planets could not be found again, since the ring plane then were aligned with the line of sight to the Earth, which of course caused a great deal of confusion. In 1655, the Dutch scientist Christiaan Huygens (1629 – 1695) was the first to describe the rings as a disk located around the planet. This sparked a 200 years long discussion if the rings were solid or made up of smaller debris. Huygens also discovered the largest moon of Saturn, Titan. The Italian astronomer Giovanni Domenico Cassini (1625 – 1712) also used the newly invented telescope to study the planets and comets of our Solar System. In the 1670's and 1680's he discovered the Saturnian moons Iapetus, Rhea, Tethys, and Dione. He also discovered the wide gap that seems to divide the main rings of Saturn, which is now named the Cassini Division in his honor.

The invention of the telescope was a great milestone in humanity's quest to understand the objects populating our Solar System. However, our hunger for knowledge drew us further and it was with the beginning of the space age, in the 1950's, that the knowledge about and exploration of our Solar System and the Universe expanded into a truly great science field. The rapid development of new technology enabled the use of artificial satellites for taking measurements that changed our view of the space around us. We finally got to know the properties of the different regions of magnetospheres, the solar wind and of the heliosphere. The most studied region is of course the magnetosphere and space environment of Earth, but today, space probes have visited and studied in situ all the planets in our Solar System. Also a number of comets, asteroids, and other celestial bodies have been thoroughly investigated. The Saturnian system was first visited by Pioneer 11, and Voyager 1 and 2. The three spacecraft passed by Saturn in 1979, 1980, and 1981, respectively, on their way further out of the Solar System. However, the planet with the magnificent ring system urged for a more extensive mission and in 1997 the Cassini spacecraft was launched. The Cassini-Huygens mission, Cassini being the spacecraft orbiter and Huygens the Titan lander, is the first mission with its main focus on Saturn and its space environment. Cassini went into orbit around Saturn

in 2004 and is still, at the time of writing, in an excellent state of health and providing us with new discoveries regarding the Saturnian system.

This thesis is a small contribution to our exploration of space, with the focus on the detailed questions that we had and have about the plasma environment of Saturn and in extension about all ring systems around gas giants. In this thesis we focus on the plasma environment around Saturn from 2.5 to 12 R_S from the center of Saturn and it is my humble hope that the reader will find satisfying answers, in this thesis, to their questions about the Saturnian plasma environment. In Chapter 2 we introduce the concepts plasma and magnetospheres. Chapter 3 gives an overview of the Cassini mission and of measurements by the instruments used for our study, especially the Cassini Langmuir probe (LP) measurements. In Chapter 4 we present the Saturnian magnetosphere with the focus on the inner plasma disk and our contribution to the investigation of this region. Chapter 5 and 6 provides a summary of our articles in English and Swedish respectively. The second part of the thesis consists of the four articles that the first part of the thesis is an introduction to.

This PhD thesis is based on and adapted from my licentiate thesis "On the structure and dynamics of the inner plasma disk of Saturn".

2. The space environment

This thesis is a contribution to our investigation of the space around us, but in order to understand our detailed studies we first need to introduce some essential concepts. This chapter gives a short introduction to the concepts of plasma, which is the form of the matter in the space around us, and the magnetosphere, which is a certain region of space surrounding a planet that has a magnetic field.

2.1 Plasma properties

Plasma is the form in which most of the directly observable matter in our Universe is, a common estimate is 99%. At Earth we seem to live in a small exception of the Universe where the plasma state is not the most common form of matter, but plasma is what surrounds us. So what is it? Well, *a plasma is defined as a quasi-neutral ionized gas that exhibits collective behavior*. *Quasi-neutrality* means that the plasma consists of roughly the same amount of positive and negative charges. This does not necessarily mean electrons and positive ions but can also include other components, such as negative ions or charged dust. Not all ionized gases are plasmas, in fact there is always a small degree of ionization in any gas. The atoms and molecules of a gas have a range of different thermal energies, and an atom or molecule is ionized when it suffers a collision of high enough energy to knock out one of its electrons. In a cold gas this does not happen frequently, since the collider must first have been accelerated to high energy by a series of favorable collisions. For instance, the density ratio between charged particles and neutrals of air at room temperature is $n_e/n_n \sim 10^{-120}$ which is not enough to have any significant effect on the behavior of the air. For an ionized gas to be a plasma it must exhibit collective behavior. The behavior of a gas is governed by collisions, the atom or molecule moves undisturbed until it collides with another atom or molecule. For plasmas the behavior is dominated by collective motions due to electric and/or magnetic fields. The motion of the charges constitutes currents and therefore also magnetic fields, which in turn will affect the motion of charges in remote regions as well. So, *collective behavior* means that the motion of the plasma is not only governed by local conditions but also by the conditions of the plasma located far away.

Stars do not only emit light, they also emit plasma particles. This stream of charged particles that is constantly emitted from our Sun is called the solar wind. The solar wind is also carrying with it the extension of the solar

magnetic field, called the interplanetary magnetic field (IMF). It is the interaction between the solar wind and a planet's magnetic field that creates the magnetosphere.

2.2 The magnetosphere

The solar wind plasma particles are emitted in all directions from the Sun and fill up our Solar System. However, if a planet has a magnetic field then this will act as an obstacle in the solar wind flow and the incoming charged solar wind particles will be deflected. This creates a different region, in the space surrounding the planet, with fundamentally different properties than the ones of the solar wind and it is this region that is the magnetosphere of the planet. Figure 2.1 shows a simplified illustration of the magnetosphere of Saturn. The orange lines illustrate the solar wind particle trajectories that are deflected by the magnetic field of the planet, illustrated by the white lines. Due to the high velocity of the solar wind a shock front, a *bow shock* (blue line), will be formed upstream of the magnetosphere. Inside of the bow shock is the *magnetosheath* (dark blue region) that contains the now much slower, but heated,

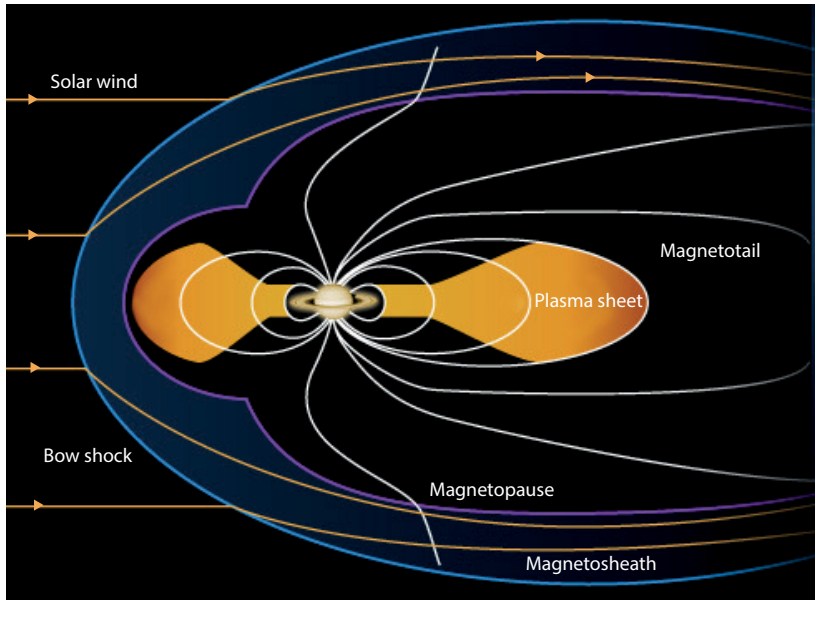

Figure 2.1. An illustration of Saturn's magnetosphere including the bow shock (blue line), magnetosheath (dark blue region), magnetopause (purple line), magnetotail, and plasma sheet (yellow region). Courtesy NASA/JPL.

solar wind particles. The interaction between the solar wind and the planetary magnetic field will create a current layer that will confine the closed planetary magnetic field to the magnetosphere. This current layer is called the *magnetopause* (purple line) and defines the outer boundary of the magnetosphere. The distance between the planet and the magnetopause, in the Sun direction, is given by the pressure balance between the solar wind dynamic pressure and the magnetic and thermal pressure found inside the magnetopause. The planetary magnetic field and the IMF may also connect to each other through magnetic reconnection. These field lines will then be referred to as open field lines as they are only connected to the planet at one point. The open field line will be forced to move along with the solar wind plasma and then eventually reconnect again in the *magnetotail*, which is the extension of the magnetosphere in the anti-Sun direction. This cyclic motion of the IMF and the planetary magnetic field reconnecting and moving trough the magnetosphere in the anti-Sun direction is called the Dungey cycle. The *plasma sheet* of Saturn is mainly filled with plasma from internal sources, such as the moons and the rings.

3. The Cassini-Huygens mission

The Cassini-Huygens mission is a collaboration between NASA, ESA, and the Italian Space Agency (Agenzia Spaziale Italiana, ASI). The design includes a Saturn orbiter, named Cassini, and a lander for the moon Titan, named Huygens. The Cassini-Huygens spacecraft was launched in October 1997 and went into orbit around Saturn in July 2004. The primary mission was set to end in 2008, but has been extended to 2017, when Cassini is scheduled to crash into Saturn in order to avoid the risk of the spacecraft contaminating any of Saturn's moons.

The main objectives of Cassini-Huygens are to study Saturn, its atmosphere, rings, moons and environment, with a special focus on the Saturnian moon Titan. An illustration of the spacecraft is presented in Figure 3.1, which also shows the location of the LP. Cassini is one of the largest interplanetary spacecraft ever built, with the spacecraft body measuring 6.7×4 m. The orbiter Cassini was developed by NASA and ASI contributed with a high-gain communication antenna, the white dish on top of the central cylindrical body. The golden dish located below the LP (Figure 3.1), is the Huygens lander. Huygens was developed by ESA with the objectives of studying the lower atmosphere and the surface of Saturn's moon Titan. Titan is of special interest not only in itself, but also because it has a very thick atmosphere that resembles the atmosphere of the early Earth. Hence, studying the atmosphere of Titan helps us understand the conditions on Earth when life was first created here. Huygens was released from Cassini in December 2004 and landed on Titan in January 2005.

3.1 The Cassini Langmuir probe

Cassini-Huygens is equipped with 18 instrument packages whereof one is the Radio and Plasma Wave Science (RPWS) instrument. The main objectives of RPWS is to study radio emissions, plasma waves, thermal plasma, and the dust in Saturn's space environment. A description of the Cassini PRWS instrument is given by Gurnett et al. (2004). Below we give a more detailed description of the RPWS Langmuir probe, which is one of the main components of the RPWS instrument package.

The LP is used to study the properties of Saturn's surrounding plasma and it consists of a titanium (Ti) sphere, 5 cm in diameter, with a titanium nitride

Figure 3.1. An illustration of Cassini, showing the location of the Langmuir probe. Given is also the location of the search coil magnetometer and the electric field antennas. Picture from "The Cassini Radio and Plasma Wave Investigation" by Gurnett et al. (2004).

(TiN) coating. The sphere is mounted at the end of a 0.8 meter long boom. The boom folds out from one of its three legs, which gives the sphere a distance of 1.5 m to the nearest spacecraft surface (Figure 3.1). To further minimize disturbances, the 10.9 cm of the boom closest to the sphere has a diameter of only 6.35 mm and is held at the same potential as the sphere. This part of the boom is also made of Ti with a TiN coating and is referred to as the stub. The rest of the boom is held at the same potential as the spacecraft, is electrically isolated from the stub and has a diameter of 9.53 mm (at the interface with the stub).

The Cassini Langmuir probe was developed by the Swedish Institute of Space Physics in Uppsala and has so far supplied us with more than 11 years of measurements from the Saturnian space environment, which have resulted in well above 100 science papers. Among these are discoveries such as dust-plasma interaction in the Kronian moon Enceladus' plume (e.g., Morooka et al., 2011), a dayside/nightside asymmetry in the ion density of the inner plasma disk (Paper II), detection of negative ions in the ionosphere of the Kronian moon Titan (e.g., Ågren et al., 2012), and a vast amount of information on the physical properties of Saturn's magnetosphere (e.g., Morooka et al., 2009; Gustafsson and Wahlund, 2010; Paper I; and Paper IV).

3.1.1 A conductor in a plasma

To properly understand the measurements performed by the Cassini RPWS/LP we first consider the simplified system of a point charge placed in a plasma consisting of only electrons and ions. A point charge placed in a plasma will cause particles of the opposite charge to position themselves like a cloud

around the point charge. This is an example of the collective behavior of a plasma that was mentioned in Section 2.1. The cloud shields out the effect of the point charge in the plasma. The shielding cloud is called a Debye sheath and it is present around every charged object placed in a plasma. The radius of the sheath depends on the properties of the plasma, it is called the Debye length and is, for singly charged electron and ions respectively, given by

$$\lambda_{e,i} = \sqrt{\frac{\varepsilon_0 k_B T_{e,i}}{q^2 n_{e,i}}} \tag{3.1}$$

where ε_0 is the electric permittivity of free space, k_B is the Boltzmann constant, $T_{e,i}$ is the plasma electron and ion temperature, respectively, $n_{e,i}$ is the plasma electron and ion number density, respectively, and q is the particle charge. The total Debye length λ_D is given by

$$\lambda_D^{-2} = \lambda_e^{-2} + \lambda_i^{-2}. \tag{3.2}$$

The Debye length also gives the electric potential φ some distance r away from the point charge,

$$\varphi = \varphi_0 \exp\left(-\frac{r}{\lambda_D}\right) \tag{3.3}$$

where φ_0 is the center potential.

Equation 3.1 shows that a larger density and smaller temperature gives a smaller Debye sheath. The peak plasma density in Saturn's inner magnetosphere is located at the orbit of the moon Enceladus at 3.95 R_S (e.g., Paper I) and the minimum plasma temperatures are found near the equatorial plane (e.g., Gustafsson and Wahlund, 2010). Hence, the smallest Debye lengths of Saturn's inner magnetosphere are found in the equatorial plane. Figure 3.2 shows the estimated equatorial Debye length for 3 to 12 R_S, a minimum value of 1.3 m are found at 4 R_S. The Debye length is important since it determines what theoretical description of the measured current that should be used. If a strong sheath is affecting the particle trajectories so that the LP probe radius $r_{LP} \gg \lambda_D$, then the Sheath Limited (SL) theory should be used to describe the measured current. This is only relevant for really dense plasmas, like, e.g., inside the ionosphere and therefore not relevant for the study presented in this thesis. On the other hand, if the probe radius $r_{LP} \ll \lambda_D$ the Orbital Motion Limited (OML) theory is used (Mott-Smith and Langmuir, 1926). Since the Cassini RPWS/LP radius is only 0.025 m we see from Figure 3.2 that OML is applicable within the studied region. This means that the screening effect is weak and the motion of a single particle is mainly governed by the probe potential and not the presence of the sheath.

If a body is placed in a plasma, where $T_i = T_e$, it will be hit by electrons much more frequently than by ions, because of the difference in thermal speed.

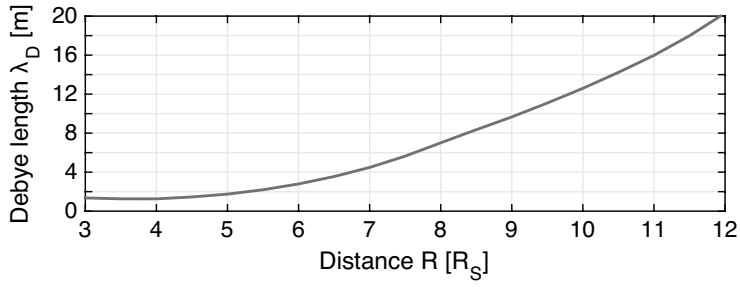

Figure 3.2. Equatorial Debye length from 3 to 12 R_S. Estimated from measured LP ion density n_i (Paper I), LP electron temperature T_e (Gustafsson and Wahlund, 2010) and CAPS ion temperature T_i (Thomsen et al., 2010).

The thermal speed is the most probable speed for a Maxwell-Boltzmann distribution and it depends on mass like

$$v_{th} = \sqrt{\frac{k_B T_{e,i}}{m_{e,i}}} \tag{3.4}$$

where $m_{e,i}$ is the electron and ion mass, respectively. Equation 3.4 shows that for equal ion and electron temperature and looking at the smallest mass difference of the ion and electron, i.e. the hydrogen ion, the electron thermal speed is at least $\sqrt{1800} \approx 42$ times larger than the ion thermal speed. This means that the frequency of electron hits will be much larger than of ion hits. The large amount of electron hits will charge the body negatively and the body will attract positive and repel negative plasma particles. If the body is a conductor, the attracted and repelled particles will cause a current to run thought the conductor. The negative charge will be built up until the conductor reaches a potential where the electron current I_e and the ion current I_i are equal, $\sum I = I_e + I_i = 0$, i.e. there is no net current (Høymork, 2000).

The Langmuir probe is a conductor so the above description is applicable, but the LP is not just passively charged but a chosen bias voltage is applied. To derive the theoretical description of how the probe current depends on the applied voltage we first need to know the velocity distribution f of the plasma particles. If we assume that the velocity distribution of the particles in a plasma is Maxwell-Boltzmann then the distribution function is given by

$$f = n_\infty \left(\frac{m}{2\pi k_B T} \right)^{3/2} \exp\left(\frac{-\frac{1}{2} m \left(v_x^2 + v_y^2 + v_z^2 \right) - q\varphi}{k_B T} \right), \tag{3.5}$$

where n_∞ is the unperturbed number density far from the probe, m is the particle mass, T is the particle temperature, v_x, v_y, and v_z are the velocities in x,

y, and z direction, q is the particle charge and φ is the potential (Laframboise and Parker, 1973). The flux to the probe is given by integrating the distribution function f times the velocity in the direction normal to the probe surface. If the distribution is isotropic, like the Maxwell-Boltzmann distribution that we have assumed, then is does not matter which velocity component we chose, we can arbitrarily select v_x. Using spherical coordinates we get

$$\begin{gathered} J = \int f v_x d^3v = n_\infty \left(\frac{m}{2\pi k_B T}\right)^{3/2} \exp\left(-\frac{q\varphi}{k_B T}\right) \times \\ \int_{v=(-2q\varphi/m)^{1/2}}^{v=\infty} \int_{\theta=0}^{\theta=\pi/2} \int_{\psi=0}^{\psi=2\pi} \exp\left(-\frac{mv^2}{2k_B T}\right) \times \\ (v cos\theta)\left(v^2 sin\theta dv d\theta d\psi\right) = n_\infty \left(\frac{m}{2\pi k_B T}\right)^{3/2} \times \\ \exp\left(-\frac{q\varphi}{k_B T}\right) \pi \exp\left(\frac{q\varphi}{k_B T}\right) \left(\frac{2\pi k_B^2 T^2}{m^2}\right) \left(1 - \frac{q\varphi}{k_B T}\right) = J_0 (1 + \chi) \end{gathered} \tag{3.6}$$

where $J_0 = n_\infty (k_B T / 2\pi m)^{1/2}$ is the random flux and $\chi = -q\varphi / k_B T$ (Laframboise and Parker, 1973). The current to the probe is obtained by

$$I = JqA_{LP} \tag{3.7}$$

where $A_{LP} = 4\pi r_{LP}^2$ is the probe surface area and r_{LP} is the Langmuir probe radius.

3.1.2 Ion and electron currents

Langmuir probe measurements may be performed in a number of different ways. The measurements used in this study are limited to voltage sweeps between +32 and -32 V. A voltage sweep means that a voltage is applied to the probe and the generated current is measured, then the next voltage is applied and the current is measured again, etc. The Cassini LP sweeps are usually performed every 10 min (so called survey mode), or every 24 s for selected flybys. Each sweep takes less that 0.5 s and gives 512 data points. The measured current is fitted to a current-voltage (I-V) curve using the OML theory (Mott-Smith and Langmuir, 1926). A typical voltage sweep is shown in Figure 3.3.

The dominant current contributors for a probe placed in a space plasma is usually the electron current I_e, ion current I_i, and photoelectron current I_{ph}, $\sum I = I_e + I_i + I_{ph}$. I_e and I_i are the currents due to the plasma particles but the photoelectron current is the due to electrons being emitted from the probe itself. The photoelectrons are being knocked out by the EUV radiation from the Sun, which is further described in Section 3.1.3. For a probe with no or negligible velocity relative to the plasma, I_e and I_i are given by equation 3.7.

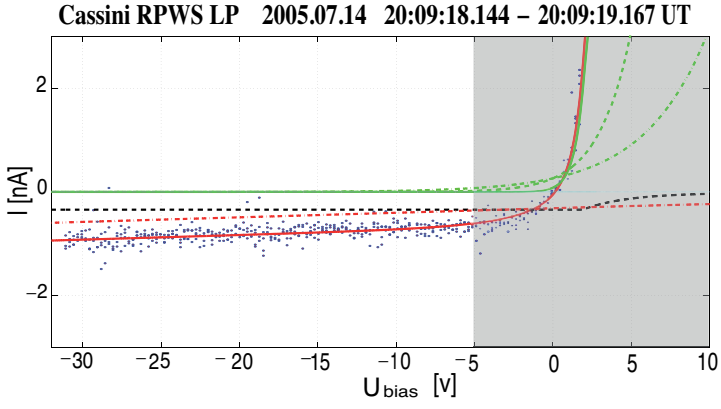

Figure 3.3. A typical voltage sweep from the RPWS/LP. The blue data points are the measured current I and the red line is the theoretical fit to the measurements. The current from one sweep is a composition of currents of different origin. The black dashed line shows the derived photoelectron current I_{ph}, the red dashed-dotted line shows the derived ion current I_i and the three green lines show three different electron currents. The graph is reduced to show -32 to 10 V (instead of -32 to 32 V) in order to put focus on the ion and photoelectron current.

For the negative voltage side the dominant current is usually the ion current that is given by

$$I_i = I_{i0}(1-\chi_i) \tag{3.8}$$

where

$$I_{i0} = -A_{LP} n_i q_i \sqrt{\frac{k_B T_i}{2\pi m_i}} \tag{3.9}$$

and

$$\chi_i = \frac{q_i(U_1 + U_{bias})}{k_B T_i} \tag{3.10}$$

where q_i is the ion charge, m_i is the ion mass, the potential $\varphi = U_1 + U_{bias}$, U_{bias} is the bias voltage to the probe and U_1 is the spacecraft potential measured at the probe (also referred to as the floating potential). For the electron current on the positive voltage side we use

$$I_e = I_{e0}(1-\chi_e) \tag{3.11}$$

where

$$I_{e0} = -A_{LP} n_e q_e \sqrt{\frac{k_B T_e}{2\pi m_e}} \tag{3.12}$$

and

$$\chi_e = \frac{q_e(U_1 + U_{bias})}{k_B T_e}. \tag{3.13}$$

A negative bias voltage applied to the probe will mainly attract the positive ions, but if an electron is energetic enough it will not be deflected by the negative potential of the probe, but pass trough and reach the probe. This current, which is present both for ions and electrons, is exponentially decreasing and will only affect the measurements for low voltages. The ion current measured for positive voltages is given by

$$I_i = I_{i0} \exp(-\chi_i) \tag{3.14}$$

where I_{i0} is given by equation 3.9 and χ_i by equation 3.10. The electron current measured for negative voltages is given by

$$I_e = I_{e0} \exp(-\chi_e) \tag{3.15}$$

where I_{e0} is given by equation 3.12 and χ_e by equation 3.13.

If there is a relative velocity component between the probe and the plasma, then equations 3.8 to 3.15 needs to be modified accordingly. When using OML the equation for the ion and electron current becomes very intricate. However, for the ion current a very convenient approximation may be used. When including a relative velocity between the probe and the ions, the ion current is given by

$$I_{i0} \approx -A_{LP} n_i q_i \sqrt{\frac{k_B T_i}{2\pi m_i} + \frac{v_i^2}{16}} \tag{3.16}$$

and

$$\chi_i \approx \frac{q_i(U_1 + U_{bias})}{\frac{m_i v_i^2}{2} + k_B T_i} \tag{3.17}$$

where v_i is the ion speed relative to the collector (Fahleson, 1967).

3.1.3 The photoelectron current

As was mentioned earlier, another large current contributor, whenever the probe is sunlit, is the photoelectron current I_{ph}. Which is due to electrons from the probe being knocked out by photons. This happens when an photon with higher energy than the work function ϕ of the material, is absorbed. For the

TiN covering the RPWS/LP the work function $\phi \approx 5$ eV which corresponds to wavelengths of $\lambda = hc/\phi \approx 250$ nm. So only radiation with wavelengths below 250 nm is able to produce photoelectrons from TiN, meaning radiation in the EUV range. If the potential of the LP is positive then some of the emitted electron will not reach very far but be collected again, if they manage to escape or not depends on their energy. If some of the photoelectrons manage to escape they will cause a small and exponentially decreasing current (which is illustrated as the exponentially decreasing photoelectron current (black dashed line) in Figure 3.3) given by

$$I_{ph} = I_{ph0} \exp\left(\frac{-q_e(U_1 + U_{bias})}{k_B T_{ph}}\right) \tag{3.18}$$

where I_{ph0} is the saturated photoelectron current and T_{ph} is the photoelectron temperature (Grard, 1973). If the probe potential is negative all of the emitted photoelectrons will be able to escape and the photoelectron current is saturated to the constant value I_{ph} (which is illustrated as the constant photoelectron current (black dashed line) in Figure 3.3), given by

$$I_{ph0} = A q_e \int_0^{\lambda_t} \Phi_\lambda Y_\lambda \, d\lambda \tag{3.19}$$

where A is the area of the sunlit probe surface, λ_t is the threshold wavelength for emission, Φ_λ is the solar flux and Y_λ is the photoelectron yield as a function of wavelength (Brace et al., 1988).

In addition to the mentioned current contributors I_e, I_i, and I_{ph}, the probe measurements are also affected by secondary electrons and ions, which are emitted due to particle hits of the spacecraft, and dust hits. However, for a larger data set, as the ones used in our studies, the current contributions from secondaries and dust are negligible (or easily corrected for).

For the study presented in this thesis, measurements from the Cassini RPWS electric antennas and the CAssini Plasma Spectrometer (CAPS) have also been used. These instruments are shortly described below.

3.2 Upper hybrid emissions

The plasma density may also be derived using measurements of upper hybrid resonance emissions by the RPWS electric antennas, which are depicted in Figure 3.1. These emissions are believed to be produced by mode conversion of electrostatic upper hybrid waves. The upper hybrid resonance frequency is given by

$$f_{uh} = \sqrt{f_c^2 + f_p^2} \tag{3.20}$$

where f_c is the electron cyclotron frequency and f_p is the electron plasma frequency.

$$f_c = \frac{eB}{m_e 2\pi} \tag{3.21}$$

where e is the elementary charge, B is the magnetic field strength, and m_e is the electron mass. The electron plasma frequency is given by

$$f_p = \frac{1}{2\pi}\sqrt{\frac{n_e e^2}{\varepsilon_0 m_e}} \tag{3.22}$$

where n_e is the electron density and ε_0 is the permittivity of vacuum. This gives that the electron density can be derived using

$$n_e \approx \left(f_{uh}^2 - f_c^2\right) / (8980)^2 \tag{3.23}$$

where f_{uh} and f_c are given in Hz, $f_c \approx 28B$, and the magnetic field strength B is given in nT. Despite the straight forward theoretical description the actual frequency spectrum can occasionally be hard to analyze, showing for example two emission lines or none at all.

3.3 CAPS

CAPS is used to measure the energy and electric charge of the plasma particles, from which particle density, velocity and temperature can be derived. CAPS is positioned on the opposite side of the large magnetometer boom and is therefore not visible in Figure 3.1. The instrument consists of three sensors mounted on a common platform. All three sensors are based on charged particle motion in electrostatic fields. As a charged particle enters a sensor the particle trajectory is dispersed in electric fields. The resulting particle trajectory is then measured using an electron-multiplier detector. The ELectron Spectrometer (ELS) measures the flux of electrons as a function of energy/charge (E/q) and entry direction. The measurements are performed within the energy range 0.7 eV to 30 keV. The Ion Beam Spectrometer (IBS) measures the flux of positive ions as a function of energy/charge (E/q) and entry direction. The measurements are performed within the energy range 1 eV to 50 keV. The Ion Mass Spectrometer (IMS) performs a similar measurement, within the same energy range, as IBS but ion species-resolved. With the IMS it is also possible to derive mass/charge (m/q).

4. The Kronian magnetosphere

Most of what was known about the Saturnian magnetosphere prior to the Cassini mission was based on measurements from flybys by the three spacecraft that passed by Saturn in the late 70's and early 80's: Pioneer 11, and Voyager 1 and 2. Even though all three provided great new insights of the physics of Saturn and its space environment, Cassini is the first spacecraft to orbit Saturn and has so far provided us with 11 years of measurements. This chapter gives an introduction to Saturn and its space environment and presents some of all the great discoveries of Cassini.

4.1 Overview

Saturn, located at $\sim$9.6 AU from the Sun, is the second largest planet in our Solar System, with a mean radius 9 times larger than the one of the Earth. Saturn also has the second largest magnetosphere (illustrated in Figure 4.1), only Jupiter's is larger. The distance of the bow shock in front of Saturn, in the Sun direction, varies with the solar wind conditions. The average value is 25 R_S, but the distance can vary between 18 and 46 R_S (Masters et al., 2008). The distance of Saturn's magnetopause, the outer boundary of its magnetosphere, is best described by a dual model with averages at 21 and 27 R_S (Kanani et al., 2010). This dual model does not correspond to variations in the solar wind but is suggested to be due to internal processes, such as mass loading and loss of the magnetospheric plasma (Achilleos et al., 2008).

The orbit of Saturn's moon Titan is located at $\sim$20.3 R_S. This means that Titan occasionally, but very rarely, is located outside of Saturn's bow shock and can then interact directly with the solar wind. When this occurs a bow shock is formed in front of Titan and a so called induced magnetosphere is created (Ness et al., 1982; Bertucci et al., 2015). This means that the solar wind particles are deflected in a magnetosheath region inside of the bow shock and current systems in the upper atmosphere of Titan creates a boundary region, the ionopause, between the IMF and the region dominated by the ionospheric plasma.

The planetary magnetic field of Saturn has a surface strength of 21 μT at the equator and is generated by its internal dynamo. The magnetic field is strictly dipole like within $\sim$6 R_S and quasi-dipolar out to $\sim$15 R_S. The ring current present outside of $\sim$6 R_S produces a small perturbation field which distorts the field (e.g., Arridge et al., 2008).

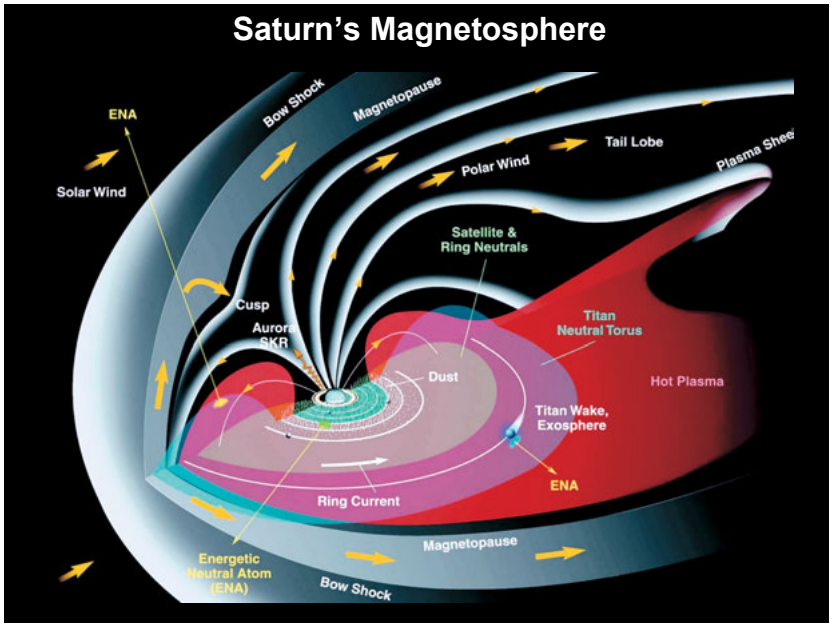

Figure 4.1. Illustration of Saturn's magnetosphere showing the magnetosheath region (gray) bounded by the bow shock and the magnetopause. Also shown is the auroral region from where the SKR are emitted, the Titan neutral torus (pink region), the orbits of some of the larger moons (white lines), and the hot plasma that is located in the magnetotail (red region). Adapted from picture from "Magnetosphere Imaging Instrument (MIMI) on the Cassini mission to Saturn/Titan" by Krimigis et al. (2004).

Saturn is known for its magnificent ring system. The main rings are located from 1.1 out to at least 8 R_S. The rings are traditionally divided into seven groups labelled from A to G and named in the order they were discovered (Figure 4.2). Today we know that the inner ring structure is not distinctly separated groups of rings but actually one large structure with a density varying with radial distance from the planet. The ring structure consists of ice and rocks ranging from nm-size up to several meters in diameter.

The rotation period of Saturn is about 10.5 h (Helled et al., 2015). Since the planet is a gas giant an exact rotation period is difficult to derive, but an estimate has be made from measuring the Saturn Kilometric Radiation (SKR). The SKR is an intense radio emission at kilometer wavelengths that is generated in the auroral region of Saturn. The power of the SKR emissions is strongly modulated by the rotation of the planet. A longitude system, called Saturn Longitude System (SLS), is defined based on the SKR emission and given by

$$\lambda_{SLS}(t,\phi) = \Phi_{SKR}(t) - \phi + 100^{\circ} \tag{4.1}$$

where ϕ is the azimuth of the observer and the phase of the SKR, Φ_{SKR}, is given by

$$\Phi_{SKR} = \Omega_{SLS}(t - t_0) \tag{4.2}$$

where t is the time of interest, t_0 is the beginning of the reference epoch (for SLS this is 00:00 h UT, 1st of January 1980) and the angular rotation speed $\Omega_{SLS} = 810.76^{\circ}$. Since the period of the SKR is varying with time, the longitude system also varies with time. The region around Saturn is also divided into a local time (LT) system where noon is pointing directly towards the Sun and midnight is in the anti-Sun direction.

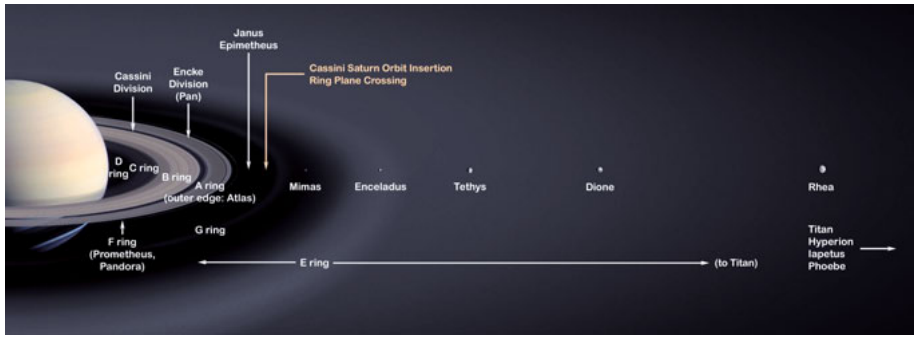

Figure 4.2. Illustration of Saturn's inner magnetosphere showing the positions of the larger moons and the main rings. Courtesy NASA

4.2 The inner magnetosphere

Saturn has 62 moons of which 13 has a diameter larger than 50 km. The studies presented in this thesis are limited to the region 2.5 to 12 R_S from Saturn. The largest moons located within this region are Mimas (at $\sim$3.07 R_S), Enceladus ($\sim$3.95 R_S), Tethys ($\sim$4.88 R_S), Dione ($\sim$6.25 R_S), and Rhea ($\sim$8.73 R_S) (Figure 4.2). The moon of most importance for the structure of the inner plasma disk is Enceladus. One of many Cassini discoveries is that Enceladus is constantly ejecting new material into its surrounding from fissures located in its south polar region (Figure 4.3) (e.g., Dougherty et al., 2006). It is mainly water vapor and condensed water that are ejected from the subsurface ocean that harbor under the icy surface of Enceladus. This water vapor plume creates a neutral torus along the orbit of Enceladus, shown as the grey region in Figure 4.2. This region is neutral dominated, with a neutral density of tens to

hundreds times the plasma density, which makes collisions with neutrals an important process. The dominant neutral species are H_2O, OH, H, H_2, and O_2. Photoionization, impact ionization of the neutrals, and subsequent transport, creates a plasma disk located around the orbit of Enceladus. The main ion components found in the inner magnetosphere of Saturn are hydrogen ions H^+ and water group ions W^+ (O^+, OH^+, H_2O^+, and H_3O^+), with some trace elements of N^+, O_2^+, and H_2^+ (e.g., Young et al., 2005).

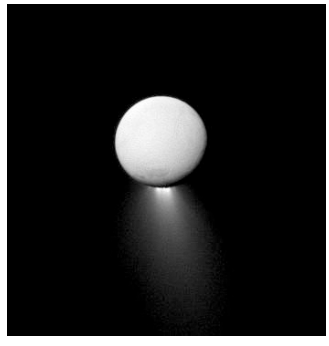

Figure 4.3. Cassini picture of Enceladus and its plume. Cassini discovered that the moon is feeding its surrounding with new material from geyser-like jets of water fed from the subsurface ocean that is located under Enceladus ice-surface. Courtesy NASA/JPL-Caltech/Space Science Institute

4.2.1 Plasma densities and temperatures

We have developed a new automatic sweep fitting routine to derive ion densities from the Cassini RPWS/LP. Previously the LP ion density could only be derived by analyzing each sweep individually requiring human supervision, which was extremely time consuming and did not result in the production of any larger data sets. Using a more general method, presented in detail in Paper I and in an improved form in Paper IV, provided the possibility of analyzing a much larger data set. The new method resulted in, among other things, the derivation of 5 years of ion density measurements, which have been used for the studies presented in Paper I, II, and III. The extended data set, 8 years of data have been used for the study presented in Paper IV. One important result is the mapping of the plasma disk structure. Figure 4.4 shows derived LP ion density from data recorded from orbit 3 to 196, corresponding to 1st of February 2005 to the 2nd of August 2013. No data from the last months of 2013 and from 2014 could be included in the analysis, due to the configuration of the Cassini orbit during this time. The periapsis of Cassini between September 2013 and December 2014 are all outside of 10.9 R_S. The measured ion density is plotted as a function of distance above the equator, Z, and distance from

the planet in the equatorial plane $\sqrt{X^2+Y^2}$, using the Saturn Solar Equatorial coordinate system.

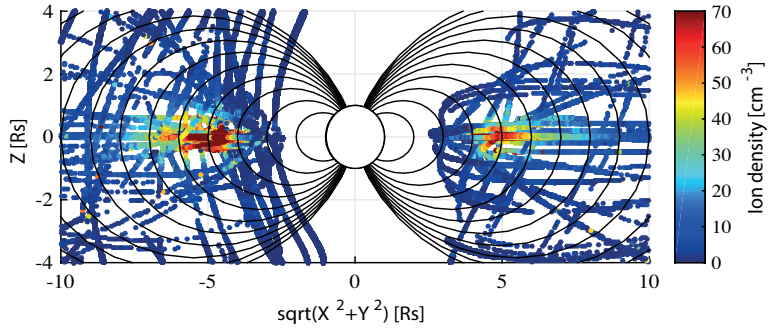

Figure 4.4. Cassini LP ion densities n_i of the inner plasma disk, derived from measurements recorded from the 1st of February 2005 (orbit 3) to the 2nd of August 2013 (orbit 196). Saturn is illustrated as the white circle centered at origo and the magnetic L shells from 2 to 12 are given as the black lines. The color scale gives the ion density up to 70 cm^{-3}. The data set is divided into a dayside (positive $\sqrt{X^2+Y^2}$ values) and a nightside (negative $\sqrt{X^2+Y^2}$ values) using the Saturn Solar Equatorial coordinate system.

A cut through the plasma disk is shown in Figure 4.5. The region around Saturn have been divided into small bins (of 0.16 R_S in the z direction and 0.09 R_S in the xy plane) and the average for each been have been estimated. Figure 4.5 shows that plasma disk densities above ~20 cm^{-3} can be found between 2.7 and 8.8 R_S with a north-south extension of ± 1 R_S.

The plasma disk density has also been estimated by an electron density model derived by Persoon et al. (2005). They used RPWS electric antenna measurements of the upper hybrid frequency f_{uh}, as described in Section 3.2. The electron density in the region 3 to 9 R_S, and within ± 0.4 R_S, was concluded to vary as $n_{e,fuh} = k\left(\frac{1}{R}\right)^{\alpha}$, where R is the radial distance from the center of the planet, $\alpha = 03.63 \pm 0.05$ and $k = 2.2 \times 10^4$ cm^{-3}. The relation $n_{e,fuh}(R)$ was derived from five equatorial orbits (Orbit B, C, 3, 4, and 5). The relation $n_{e,fuh}(R)$ was used in Paper I to show a good agreement between the LP n_i and $n_{e,fuh}$ for densities above 20 cm^{-3}. Persoon et al. (2005) also shows a great variation in electron density profile within 5 R_S, even varying between the inbound and outbound portion of the same orbit. An updated study of electron densities derived from f_{uh} was presented by Persoon et al. (2013). They used 7 years of data, recorded within $\pm 8^\circ$ of the magnetic equator, which provided the relation

$$n_{e,fuh} = \frac{n_0}{\frac{1}{2}\left(\left(\frac{4.6}{R}\right)^4 + \left(\frac{R}{4.6}\right)^{4.8}\right)} \tag{4.3}$$

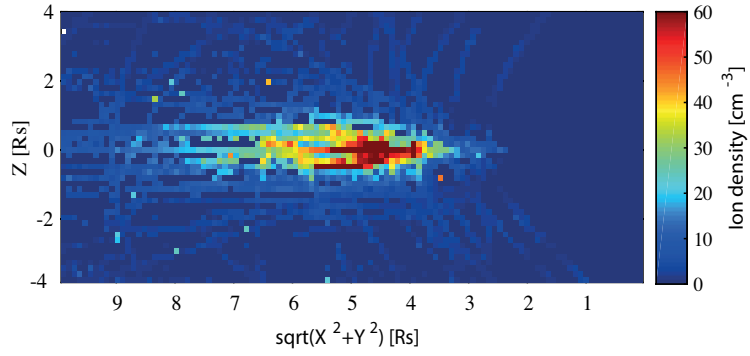

Figure 4.5. Cassini LP ion densities n_i of the inner plasma disk, derived from measurements recorded from the 1st of February 2005 (orbit 3) to the 2nd of August 2013 (orbit 196). The figure shows a cut through the plasma disk derived from average of all data recorded for each bin. Each bin is 0.16 R_S in the z direction and 0.09 R_S in the xy plane. Saturn is centered at origo to the right in the figure. The color scale gives the ion density up to 60 cm^{-3}. No division between dayside values and nightside values have been made.

where $n_0 = 72$ cm^{-3} is the average peak density of the plasma disk (excluding the near vicinity of Enceladus), and R is the radial distance from the planet in the equatorial plane. The peak density $n_0 = 72$ cm^{-3} is usually located between 4 and 5 R_S, with the best fit at 4.6 R_S (Persoon et al., 2013).

As stated in Section 3.3, the plasma density may also be derived from measurements performed by the CAPS instrument. Thomsen et al. (2010) presented ion densities derived from the first 4.5 years of CAPS measurements, outside of 6 R_S and within $\pm 5^\circ$. They found that the ion density $n_{i,C}$ is varying as $n_{i,C} = 627\exp(-0.517L)$ (red line of Figure 4.6) or $n_{i,C} = 1.38 \times 10^6 L^{-5.68}$ (yellow line of Figure 4.6). Figure 4.6 shows all the above presented plasma density fits compared to the LP ion density recorded within ± 0.5 R_S in the z direction. The black line shows the fit derived from the LP n_i given by

$$n_i = \frac{n_0}{\frac{1}{2}\left(\left(\frac{4.44}{R}\right)^{8.20} + \left(\frac{R}{4.14}\right)^{3.44}\right)}. \tag{4.4}$$

where $n_0 = 72$ cm^{-3}. The best agreement with the LP n_i is with the fits from Persoon et al. (2005) (green line) and Persoon et al. (2013) (purple line). The best agreement is expected to be with the green line since this corresponds best to the chosen LP region (within ± 0.5 R_S). Persoon et al. (2013) use $\pm 8^\circ$, which corresponds to ± 1.4 R_S (in the z direction) at 10 R_S. Inspecting Figure 4.5 shows that this will include a large amount of very low density plasma. Apart from this outer region, the fit from Persoon et al. (2013) (purple line)

agrees well with the LP n_i. Thomsen et al. (2010) use $\pm 5^\circ$, which corresponds to ± 0.9 R_S (in the z direction) at 10 R_S.

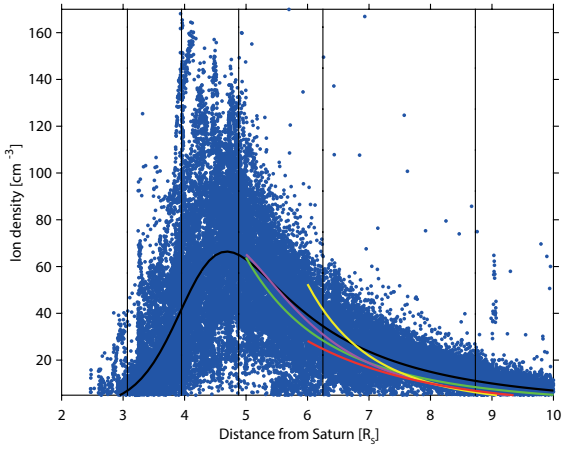

Figure 4.6. Cassini LP n_i, derived from measurements recorded from orbit 3 to orbit 196 and within ± 0.5 R_S of the equator. Included is the fit to the LP n_i (black line), CAPS ion density $n_{i,C}$ (red and yellow lines), and the f_{uh} electron density (green and purple lines).

Shippers et al. (2013) also investigated the structure of electrons in the inner magnetosphere from 2.8 to 10 R_S, using measurements from July 2004 to May 2012. They used the quasi-thermal noise spectroscopy method, based on HF power spectra measurements from the RPWS instrument, to show that the results could be divided into two regions. The inner region is located around the orbit of Enceladus, 3-5 R_S, and is characterized by a large variety in the measured electron density and an increasing core temperature. The outer region, 5 to 10 R_S, has a decreasing electron density ($\propto R^{-4.19}$) and a small decrease in core temperature ($\propto R^{-0.3}$). Shippers et al. (2103) also found a local time asymmetry in the electron density and temperature. This will be discussed further in Section 4.2.4. Gustafsson and Wahlund (2010) used RPWS/LP measurements to derive the equatorial electron temperature in the radial region 2.5 to 7 R_S. They showed that the temperature varies as

$$T_e = (0.04 \pm 0.02) L^{2.8 \pm 0.4}, \tag{4.5}$$

i.e., ranging from $\sim$0.5 to $\sim$9.3 eV. A similar dependence was derived by Schippers et al. (2013), giving

$$T_e = 0.03 L^{2.7 \pm 0.1} \tag{4.6}$$

for the region 2.8 to 4.8 R_S. Gustafsson and Wahlund (2010) also showed that the electron temperature is increasing with latitude. For L = 4, $T_e(z)$ is given by

$$T_e = (2.3 \pm 0.7) \exp(z^2 / H_{Te}^2) \tag{4.7}$$

where $H_{Te} \approx 0.8 \pm 0.1$ R_S, i.e., ranging from ~2.3 eV (at $\lambda = 0°$) to ~6.3 eV ($\lambda = 12°$).

Thomsen et al. (2010) also presented ion temperature T_i derived from 4.5 years of CAPS data. The estimated water group W^+ ion temperature range from 40 eV at 6.5 R_S to 200 eV at 12 R_S, and the hydrogen H^+ ion temperature range from 12 eV at 6.5 R_S to 18 eV at 12 R_S. The W^+ temperature estimate are used to derive the error in the LP ion density and velocity due to an omitted thermal energy term in the derivation, see Paper I Section 4. More recent investigation of the ion temperature shows a dayside/nightside asymmetry of 20-30 eV in the region 6-7 R_S (Thomsen et al., 2012). This is further discussed in Section 4.2.4.

4.2.2 Ion velocities

Our new method to analyze LP data also included a derivation of the ion drift velocity of the bulk ion population. The LP cannot separate the velocity components, it only measures the magnitude of the velocity. Since the dominant velocity component near the equator plane is the azimuthal velocity (e.g., Sittler et al., 2006; Thomsen et al., 2010), in the corotational direction, an estimate of equatorial ion velocity can still be made. The first estimate, using the 5 years data set, was presented in Paper I, and an update, using the 8 years data set, was presented in Paper IV. The estimated azimuthal ion velocity $v_{i,\theta}$ is presented in Figure 4.7.

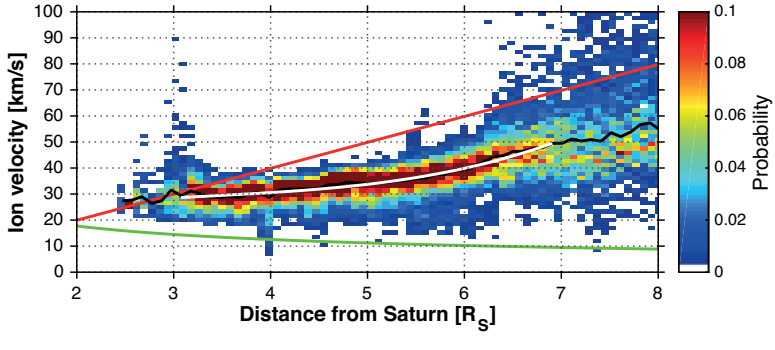

Figure 4.7. Cassini LP $v_{i,\theta}$ derived from measurements recorded from orbit 3 to orbit 196 and within ±5 R_S of the equator. The radial region and the velocity interval are divided into small bins (0.08 R_S and 1.6 km/s) and the probability of measuring a certain velocity for each radial region is given by the color bar. Included is the corotation speed (red line), Keplerian speed (green line), the median velocity for each radial bin (black line) and the best fit to $v_{i,\theta}$ in the region 3 to 7 R_S, which is given by the polynomial $v_{i,\theta} = 0.3R_S^3 - 3.1R_S^2 + 12.6R_S + 10.6$.

The ions of the inner plasma disk are mainly created from impact ionization, and photoionization of the neutrals, and from ion-neutral charge exchange. This means that new ions start with Keplerian speed, in average, which is the speed of the neutrals,

$$v_k = \sqrt{\left(\frac{GM_S}{r}\right)} \tag{4.8}$$

where G is the gravitational constant, M_S is the mass of Saturn, and r is the distance from Saturn. The Keplerian speed is given by the green line in Figure 4.7. A new ion will directly be subject to the force exerted by the magnetic and electric fields, the Lorentz force. This will, in the absence of collisions, force the ion to gyrate around the magnetic field line in the plasma rest frame. The acceleration of the new ions constitute a current system, known as corotation enforcement currents, which moves radial outwards and close in the ionosphere of Saturn through field aligned currents. The current system is illustrated in Figure 4.8. The newly produced ions are "picked-up" by the magnetic field, which would ideally cause the ions to corotate with the magnetic field. The corotation speed is given by the red line in Figure 4.7. Figure 4.7 shows that the velocity is deviating from co-rotation at 3.2 R_S. The subcorotation has also been detected by the CAPS instrument (e.g., Wilson et al., 2009; Thomsen et al., 2010) and by the Voyager 1 and 2 measurements (e.g., Richardson, 1986). Several reasons have been suggested to be the cause of the subcorotation; inertial drag associated with the production of new ions, and

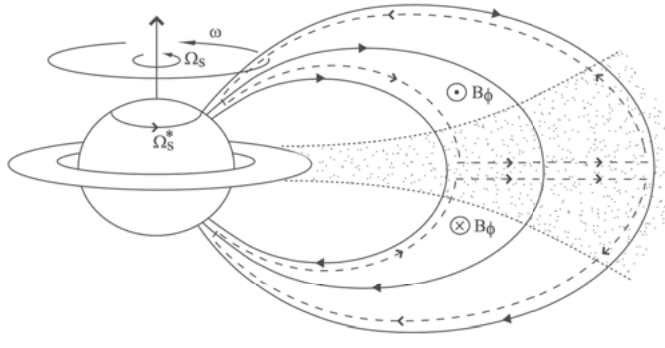

Figure 4.8. Illustration of the corotation enforcement currents (arrowed dashed lines) in the Saturnian magnetosphere. The radial currents close in the ionosphere of the planet through field aligned currents. The radial currents are also associated with the azimuthal field components B_ϕ, which bends the planetary magnetic field lines in the azimuthal direction. Ω_S is the angular velocity of Saturn, ω is the angular velocity of a chosen shell of field lines, and Ω_S^* is the angular velocity of the neutral upper atmosphere. Figure from Cowley and Bunce (2003).

radial outward transport of the plasma, (e.g., Hill, 1979; Saur et al., 2004) and coupling between charged dust and the plasma (Wahlund et al., 2005). Hill (1979) estimated the corotation lag within the Jovian magnetosphere and showed that the viscous torque, associated with ion-neutral collisions in the atmosphere required subcorotation. They derived an expression for the distance at which subcorotation starts given by

$$D_0 = (\pi \Sigma R_p^2 B_p^2 / \dot{M})^{1/4} \tag{4.9}$$

where Σ is the height-integrated Pedersen conductivity of the atmosphere, R_p is the planetary radius, B_p is the planetary surface magnetic field strength, and $\dot{M}$ is the total rate of outward transport and production of plasma. Which shows that a small conductivity in the atmosphere and a large $\dot{M}$ is important for a significant subcorotation. (Saur et al., 2004) use equation 4.9 and estimate a subcorotation starting in between 3 and 4 R_S.

4.2.3 A varying plasma source

When we first discovered a dayside/nightside asymmetry in the ion density we wanted to make sure that it was not just an apparent asymmetry due to the configuration of the Cassini orbits. For example, simulations by Cassidy and Johnson (2010) have shown that the neutral density (mainly H_2O, OH, and O) shows a characteristic "banana" shaped increase centered around Enceladus (see left panel Figure 4.9). If the plasma density showed the same type of increase close to Enceladus and the Enceladus flybys where mainly located closer to LT midnight, then this would cause an apparent correlation between LT midnight and an increase in plasma density. However, the same "banana"

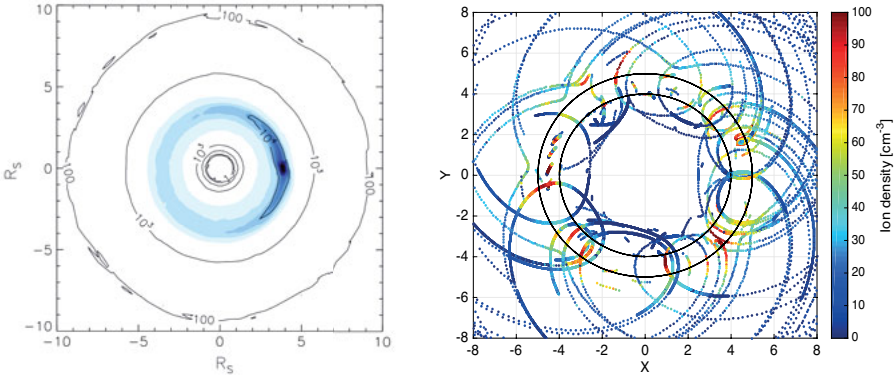

Figure 4.9. Left panel: Simulated neutral densities (H_2O, OH, and O) from Cassidy and Johnson (2010). Enceladus is fixed at y = 0 and x = 3.95 R_S. Right panel: Ion density measured by the LP. Enceladus is fixed at y = 0 and x = 3.95 R_S.

shaped density increase cannot be find in the plasma density as shown in the right panel of Figure 4.9. This shows that the closeness to Enceladus cannot have an effect on the plasma density, at least not for larger distances. However, the region very close to Enceladus shows in increase in plasma density (Figure 4.10). This is a very small region and could not give rise to the detected dayside/nightside asymmetry.

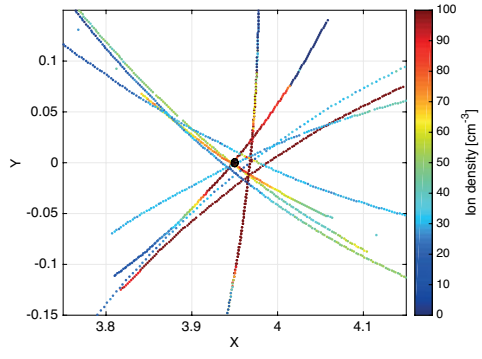

Figure 4.10. Ion density measurements in the near vicinity of Enceladus. Enceladus is illustrated as the black dot fixed at y = 0 and x = 3.95 R_S.

Observations by the Cassini Visual and Infrared Mapping Spectrometer (VIMS) show that the brightness of Enceladus' plume varies with the distance between Enceladus and Saturn (Hedman et al., 2013). The plume brightness is strongest at apoapsis and weakest at periapsis. This implies that more material is escaping the plume when Enceladus is further away from Saturn and the fissures in the ice surface of Enceladus are under more tension due to tidal stresses (Hedman et al., 2013). If the Cassini orbit passes of LT midnight happened to coincide with apoapsis passes of Enceladus, an apparent correlation between LT midnight and higher densities would be visible. However, the LT midnight passes do not correlate with the apoapsis passes of Enceladus and the same increase in ion density as in brightness cannot be detected. We investigated this using the electron density n_e derived from f_{uh} recorded during 8 orbits when Cassini passed near (within ± 0.1 R_S of) Enceladus. The electron density vs. the distance Enceladus-Saturn is shown in Figure 4.11. Figure 4.11 shows that the largest n_e value at apoapsis (3.97 R_S) is a factor of 2 larger than the largest value recorded closer to periapsis (3.93 R_S). However, a large amount of low density values are also present at apoapsis. One could argue that this might be due to the changing activity level of the moon over the years and that if more measurements were recorded at periapsis during the early years of the Cassini mission, Figure 4.11 would show a broad band of densities but still with the trend of increasing densities for increasing distance. The measured electron density data from the orbit pairs 3, 4, 88, 91, and 120,

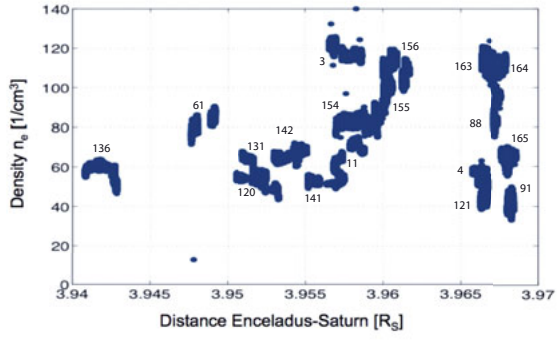

Figure 4.11. Electron density measurements in the near vicinity of Enceladus ($\pm$0.1 R_S). The number states during which orbit the data was recorded. Direct plume passages are removed.

121 are, however, contradicting this argument. A likely explanation that the plume variation can not be seen in the electron density data is that other effects are causing the plasma disk density to vary with a greater variation than the one caused by the varying plume.

4.2.4 Dayside/nightside asymmetry

One of the main results from Paper I is that for any chosen radial region a broad range of plasma densities are measured. E.g., at the orbit of Tethys (at 4.88 R_S) the measured density ranges from $\sim$15 cm^{-3} to $\sim$130 cm^{-3}, the expected variation due to the errors of the derivation method is 20 cm^{-3} (for estimates of and a discussion of the measurement error see Paper II). The wide range of measured ion densities was interpreted as caused by a spatial or temporal variation of the plasma disk. This motivated the work presented in Paper II.

A number of studies have shown the presence of a dayside/nightside asymmetry in various parameters related to the inner plasma disk; Andriopoulou et al. (2012) and Andriopoulou et al. (2014) showed that energetic electron microsignatures, related to the absorption of charged particles by the icy moons, were displaced outwards from Saturn around LT noon and inward around LT midnight; Thomsen et al. (2012) showed a dayside/nightside asymmetry in ion and electron temperature and in phase space densities; and Wilson et al. (2013) showed LT asymmetries in ion velocities. A LT asymmetry was also found in the ion density and in the azimuthal ion velocity, Paper II. We suggest that this asymmetry is due to shifted particle orbits, which could be due to the radiation pressure force. However, shifted particle orbits should result in a shifted plasma disk. The RPWS/LP measurements show higher ion densities on the nightside in between 4 and 6 R_S, but not higher densities in the dayside for larger radial distances which would be expected (Figure 4.12). However,

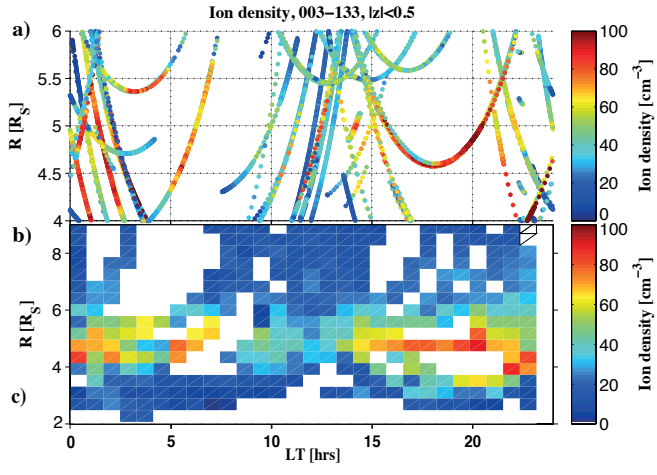

Figure 4.12. The LP ion density derived from 5 years of data. Panel a shows the individual data points measured in between 4 and 6 R_S given as a function of LT from 0 to 24 hours. Panel b shows the radial, from 2 to 9 R_S, and LT region divided into smaller bins (0.4 R_S and 0.8 h) and the average ion density value for each bin given by the color bar.

this is detected by the density estimates by Schippers et al. (2013) (Figure 4.13) and by CAPS measurements (R. Wilson, personal communication, 2014). A likely explanation that higher densities on the nightside cannot be seen for larger radial distance than 6 to 7 R_S in Figure 4.12 is the lack of LP data coverage in this region.

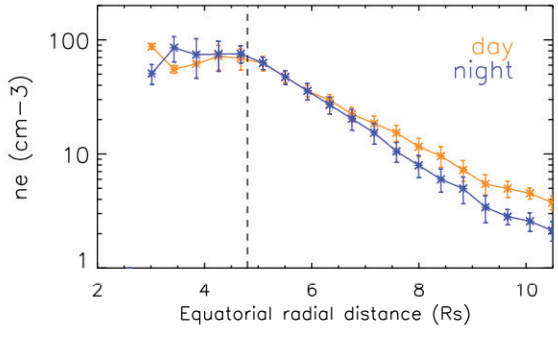

Figure 4.13. Equatorial electron densities, $|z| < 0.05$ R_S, derived from RPWS f_{uh} measurements from July 2004 to May 2012. The dayside densities are recorded within LT 7-17 h (yellow) and nightside within LT 19-5 h (blue). Figure from Schippers et al. (2013).

Another plasma variation that has also been investigated is the plasma density modulation reported by Gurnett et al. (2007). They used electron densities $n_{e,fuh}$ from 14 equatorial orbits, $|z|$ <0.1 R_S, from the 1st of July 2004 to the 1st of July 2006 and showed that $n_{e,fuh}$ varies with the Saturn Longitude System (SLS), which is based on the SKR emission as stated by equation 4.1. The derived modulation is shown in Figure 4.14, which shows electron densities varying from 40 to 90 cm^{-3}. The varying electron density was suggested to be due to a two cell convection pattern driven by a centrifugal instability and fixed in SLS. We used the LP ion density recorded in the same region and time interval as the $n_{e,fuh}$ presented in Figure 4.14 and could reproduce the density modulation presented by Gurnett et al. (2007). The ion density as a function of SLS4 (the fourth version of the SLS system) south (from the south component of the SKR emission) are presented in Figure 4.15. However, the extended data set, all LP ion density data recorded from orbit 3 to 133 (5 years of measurements) do not show the same modulation. Figure 4.16 shows the 5 years of LP ion density data versus SLS4 south. Since no updated study of the $n_{e,fuh}$ modulation has been published and the result presented in Figure 4.16 showed no modulation, a possible n_i SLS dependence was not further studied.

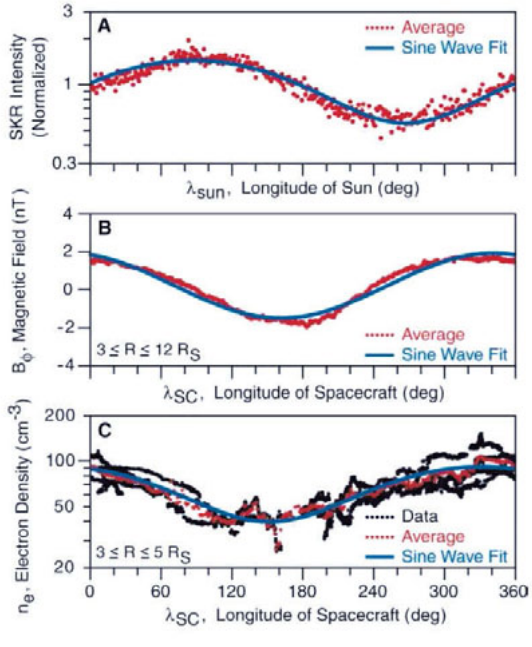

Figure 4.14. Panel A: the normalized SKR intensity vs. longitude. Panel B: The B_ϕ component of the magnetic field vs. longitude. Panel C: Equatorial electron densities $n_{e,fuh}$, $|z|$ <0.1 R_S, derived from RPWS f_{uh} measurements from 14 orbits from the 1st of July 2004 to the 1st of July 2006, vs. longitude. $n_{e,fuh}$ varies with nearly a factor of 2. Figure from Gurnett et al. (2007).

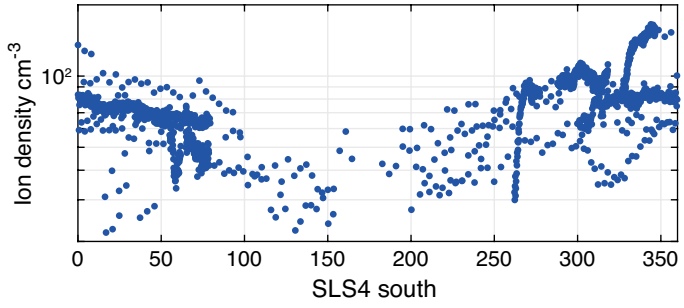

Figure 4.15. Equatorial ion densities n_i, $|z|$ <0.1 R_S, from 14 orbits from the 1st of July 2004 to the 1st of July 2006 versus SLS4 south. n_i confirms the density modulation derived by Gurnett et al. (2007).

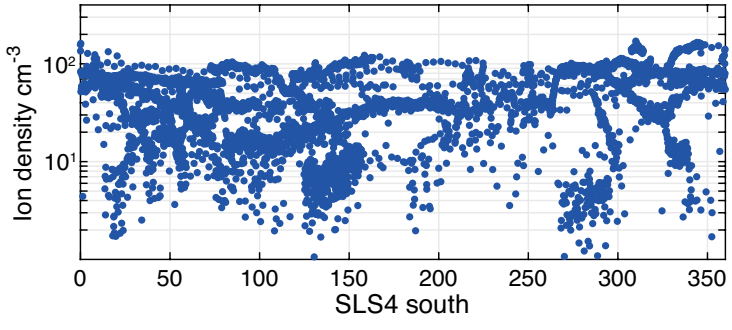

Figure 4.16. Equatorial ion densities n_i, $|z|$ <0.1 R_S, from orbit 3 to 133 versus SLS4 south. No density modulation can be detected.

4.2.5 Transport and chemical loss rates

A study showing that loss by recombination dominates over the loss by transport presented by Fleshman et al. (2013) and ideas that the ionization of neutrals showed a LT asymmetry (F. Crary, personal communication, 2014) sparked the idea of using the LP probe measurements to investigate the importance of ion loss by chemistry and by transport. The study is presented in Paper III. We use an expression for the latitude dependence of the ion density $n_i(L,\theta)$ from a model presented by Persoon et al. (2009) based on electron densities derived from upper hybrid frequency measurements from more than 50 orbits. $n_i(L,\theta)$ is derived from the centrifugal force term of the magnetic field-aligned force equation. We show that the $n_i(L,\theta)$ relation also describes the LP ion density well. This means that the potential problem of underestimating the plasma density derived from electron density measurements, due to the possibility of

a significant amount of electrons being attached to dust grains, is not relevant for our studied region.

We use $n_i(L,\theta)$ to derive the total fluxtube content. The magnetic flux ϕ is constant along a field line, for a certain L shell of width ΔL.

$$\phi = BA\Delta L = constant \tag{4.10}$$

where B is the magnetic field strength and A is the area. By the equator

$$\phi = \frac{B_0}{L^3} 2\pi R_S^2 L\Delta L. \tag{4.11}$$

For a dipole magnetic field B is given by

$$|\mathbf{B}| = |-B_0(R_S^3/r^3)(2\sin\lambda + \cos\lambda)| = B_0(R_S^3/r^3)(4-3\cos^2\lambda)^{1/2} \tag{4.12}$$

where B_0 is the surface magnetic field strength and λ is the latitude. Using the field line equation

$$L = \frac{r}{\cos^2\lambda} \tag{4.13}$$

equation 4.12 can be rewritten as

$$B = \frac{B_0(1+3\sin^2\lambda)^{1/2}}{L^3\cos^6\lambda}. \tag{4.14}$$

The equation for the line segment ds along a dipole field line is given by

$$ds = L\cos\lambda\,(1+3\sin^2\lambda)d\lambda \tag{4.15}$$

which we use to derive the total volume of a fluxtube of width ΔL. The volume is given by

$$V = 2\int_0^{s_{max}} A\Delta L ds = 2\int_0^{s_{max}} \frac{\phi}{B} ds \tag{4.16}$$

Rewriting the volume to co-latitude θ (θ = *pi*/2-λ), using the width $\Delta L = 1$, and inserting equations 4.11, 4.14, and 4.15 we get

$$V = 4\pi R_S^3 L^2 \int_{\theta_{min}}^{\pi/2} \sin^7\theta \; \mathrm{d}\theta \tag{4.17}$$

which we use to derive the total number of ions per unit L shell

$$N = 4\pi R_S^3 L^2 \int_{\theta_{min}}^{\pi/2} n_i(L,\theta)\sin^7\theta \; \mathrm{d}\theta \tag{4.18}$$

Our total flux tube content estimate agrees well with the estimate by Sittler et al. (2008), derived from CAPS data recorded during SOI, within 8 R_S. $n_i(L,\theta)$ is also used to derive the ion loss rate by dissociative recombination, which is the dominant loss process in the inner plasma disk (Fleshman et al., 2010). The derived chemical loss rate is compared to a conservative estimate of the radial ion velocity, which shows that transport loss rate dominate chemical loss rate in all of the plasma disk (Paper III).

5. Summary of publications

5.1 Paper I: *Ion densities and velocities in the inner plasma torus of Saturn*

Authors: M.K.G. Holmberg, J.-E. Wahlund, M.W. Morooka, and A.M. Persoon

Journal: Planetary and Space Science

Status: Published

This paper presents ion densities and ion velocities derived from RPWS/LP measurements. The measurements are used to study the structure and dynamics of the inner plasma disk of Saturn. The studied region is limited to 2.5 to 12 Saturn radii (1 R_S = 60,268 km) and the data is recorded during the time period from orbit 3 to 133, which corresponds to the 1st of February 2005 to the 27th of June 2010. The investigation showed that the dominant part of the plasma torus, ion densities above $\sim$15 particle/cm^3, is located in between 2.5 and 8 R_S from the planet, with a north-southward extension of $\pm$2 R_S. The derived plasma disk ion density shows a narrow density maximum at the orbit of Enceladus (at 3.95 R_S), which corresponds to direct plume passages, with a measured ion density of up to 10^5 cm^{-3}. Outside of the plume a broad density maximum is found in between the orbits of the moons Enceladus and Tethys (at 4.88 R_S), with an average peak density at 4.6 R_S. Ion density values vary between 20 and 125 cm^{-3} at the location of the density maximum. The error of the derivation method is expected to introduce a density variation of $\sim$20 cm^{-3}, so the additional density variation is interpreted to be due to the dynamics of the plasma disk. The equatorial ion density structure, limited to $|z|$ <0.5 R_S, shows a slower decrease away from Saturn than towards. The outward decrease is well described by the relation $n_{eq} = 2.2 * 10^4 (1/R)^{3.63}$, a relation derived from electron density measurements by Persoon et al. (2005). A less prominent density peak, that the clear density peak of the Enceladus' plume, of 115 cm^{-3} is detected at the orbit of Tethys. This could be an indication of particle sputtering from or active vents on Tethys. Density peaks are not recorded at the location of the orbits of the moons Mimas, Dione, and

Rhea. An estimation of the azimuthal ion velocity $v_{i,\theta}$ is also presented. $v_{i,\theta}$ shows a clear general trend in the region between 3 and 7 R_S, described by $v_{i,\theta} = 1.5R^2 - 8.7R + 39$. Outside of this region the measurements are to close to the noise level of the instrument to produce a reliable estimation of $v_{i,\theta}$. The average $v_{i,\theta}$ starts to deviate from corotation speed at around 3 R_S and reaches down to $\sim$68 % of corotation close to 5 R_S.

My contribution: I performed the data analysis together with the co-authors. I carried out the study and wrote most of the text.

5.2 Paper II: *Dayside/nightside asymmetry of ion densities and velocities in Saturn's inner magnetosphere*

Authors: M.K.G. Holmberg, J.-E. Wahlund, and M.W. Morooka

Journal: Geophysical Research Letters

Status: Published

This paper presents an extended study of the inner plasma disk of Saturn. Paper I showed that the Cassini RPWS/LP measures a broad range of the ion densities for any chosen radial distance. This density variation could partly be explained by the here presented dayside/nightside asymmetry, which is detected in both ion density and velocity. We present Cassini LP ion density and velocity measurements from orbit 3 to 133, the same data set as was used for the study presented in Paper I, i.e. measurements recorded after equinox are also included. The data show a clear dayside/nightside asymmetry in the radial region 4-6 R_S from the center of Saturn. The measured ion densities n_i variation ranges from an average of $\sim$35 cm^{-3} for the dayside values close to noon up to $\sim$70 cm^{-3} for the nightside values around midnight. The measured azimuthal ion velocities $v_{i,\theta}$ variation ranges from $\sim$28-32 km/s for the dayside values around noon to $\sim$36-40 km/s for the nightside values around midnight. This results in an azimuthal ion velocity difference between noon and midnight of $\Delta v_{i,\theta}$ $\sim$5-10 km/s. Wilson et al. (2013) used CAPS data to study the radial ion velocity and found an additional velocity component directed from dusk to dawn, causing an asymmetry in the dawn/dusk ion radial velocities of $\sim$3-10 km/s. An additional velocity component in the dusk to dawn direction would correspond to higher nightside and lower dayside azimuthal velocities. The additional velocity component found in the azimuthal ion velocities $v_{i,\theta}$ of $\Delta v_{i,\theta}$ $\sim$5-10 km/s would therefore correspond to the additional radial velocity

component of ∼3-10 km/s. The slightly larger LP velocity difference could be explained by a recently detected dayside/nightside ion temperature asymmetry (Thomsen et al., 2012), which would result in a velocity difference of ∼4 km/s at 6.5 R_S. Measurements of and near the Enceladus' plume have shown that large amount of negatively charged nm-sized dust are ejected from the plume (Jones et al., 2009; Hill et al., 2012). If the densities of negatively charged nm-sized grains is large also in the rest of the plasma disk, then this will have a noticeable effect on the dynamics of the plasma disk. We suggest that the detected dayside/nightside asymmetry is due to the radiation pressure force acting on the negatively charged nm-sized dust of the E-ring. The radiation pressure force will introduce an extra grain and ion drift component, directed from dusk to dawn, equivalent to the force of an additional electric field of 0.1-2 mV/m for a 10-50 nm sized grain. The additional drift component can explain the dayside/nightside asymmetry of the azimuthal ion velocity as well as the dawn/dusk asymmetry found in the radial velocity. The additional drift component due to the radiation pressure force can also explain the asymmetry of the ion density, since the ions will be pushed outwards in their orbit as they move from the nightside towards the dayside and pushed inwards as they move from the dayside to the nightside. This will create a shift, towards the Sun, in the particle orbit and therefore also in the plasma disk density.

My contribution: I planned and carried out the study. I performed the data analysis together with the co-authors. I wrote the text.

5.3 Paper III: *Transport and chemical loss rates in Saturn's inner plasma disk*

Authors: M.K.G. Holmberg, J.-E. Wahlund, E. Vigren, F. Bagenal, T. A. Cassidy, D.J. Andrews

Journal: Journal of Geophysical Research

Status: Submitted

This paper presents an investigation of ion losses, due to outward radial transport and chemical loss by recombination, in Saturn's inner plasma disk. We use the same ion density data set as was use in Paper I and II. We show that the relation for $n_i(\theta)$, where θ is the co-latitude ($\theta = \pi/2 - \lambda$, λ is the latitude), derived by Persoon et al. (2009) from electron density estimates, also describes the LP ion density n_i well. Earlier comparisons of electron and ion densities have shown a discrepancy, $n_i > n_e$, in the near vicinity of Enceladus (Morooka

et al., 2011), which could be explained by a significant number of the electrons being attached to dust grains. The good agreement between $n_e(\theta)$ and $n_i(\theta)$ shows that this is not a problem in our studied L shell region. The total flux tube content NL^2 for the L shells 2.5 to 10 is also derived and shown to vary as

$$NL^2 = \frac{7.93 \times 10^{33}}{\frac{1}{2}\left(\left(\frac{4.51}{R}\right)^{8.47} + \left(\frac{R}{8.14}\right)^{0.32}\right)} \tag{5.1}$$

where R is the equatorial radial distance from the planet. The derived NL^2 agrees well with earlier estimate by Sittler et al. (2008), who used CAPS data from Saturn Orbit Insertion (SOI), within L shell 8. The total ion source rate is derived to 5.8×10^{33} particles/s for L shell 4 to 10. A net mass loading rate of 123 kg/s for L shell 4 to 10, is also derived, and 126 kg/s for L shell 2.5 to 10. Of the total mass loading rate, the water group ions W^+ accounts for 120 kg/s and the hydrogen ions H^+ accounts for the remaining 3 kg/s, for L shell 4 to 10. The total plasma content for L shell 4 to 10 is derived to 1.9×10^{33} ions. This agrees well with the estimate of 2×10^{33} derived by Rymer et al. (2007) using CAPS measurements and RPWS electric field spectrums. A conservative estimate of the radial transport times τ is used to derive the transport loss rate. The radial transport time τ is derived from a model by Fleshman et al. (2013) based on CAPS data presented by Wilson et al. (2008). The chemical loss of ions is dominated by dissociative recombination between OH^+, H_2O^+, H_3O^+, and electrons. The derived loss by transport and by dissociative recombination show that the outward radial transport dominates over chemical loss between L shell 2.5 and 10. However, chemical loss may still have an impact on the structure of the plasma disk in the region closest to Enceladus at 3.95 R_S ($\sim \pm$ 0.5 R_S). In this region transport loss and chemical loss only differ with a factor 2.7-3.2 for the total ion population. We also derive the ion production rate P which ranges from 2.6×10^{-5} $cm^{-3}s^{-1}$ (at L = 10) to 1.1×10^{-4} $cm^{-3}s^{-1}$ (at L = 4.8).

My contribution: I planned the study and performed the data analysis together with the co-authors. I carried out the study. I wrote most of the text.

5.4 Paper IV: *Density structures, ion drift speeds, and dynamics in Saturn's inner plasma disk*

Authors: M.K.G. Holmberg, O. Shebanits, J.-E. Wahlund

Journal: Journal of Geophysical Research

Status: To be submitted

We use an extended LP data set from the 1st of February 2005 (orbit 3) to the 2nd of August 2013 (orbit 196) to investigate the structure and dynamics of the inner plasma disk of Saturn. We show that the density maximum of the plasma disk, excluding the direct flybys of the Enceladus plume, is located in between 4.5 and 4.8 R_S. The previously reported large density variation is confirmed, showing a variation of one order of magnitude for the innermost part of the plasma disk and decreasing outwards. This indicates an internal source of the density variation and not an external source located outside of the inner plasma disk. Ion densities shows higher nightside values than dayside values, differing with a factor of up to 3.3 in the region 3.3 to 4.7 R_S. Our study shows that the main variability of the plasma disk is due to the dayside/nightside density asymmetry. We present a large ion velocity difference between dayside and nightside values outside of 6.5 R_S, with a difference of up to a factor of 2.2. The large velocity difference is suggested to be due to a large radial velocity component present in the nightside plasma disk region and/or larger ion temperature asymmetries. We also confirm the seasonal dependence of the innermost part of the plasma disk, previously reported by Persoon et al. (2015).

My contribution: I planned the study. I carried out the study and performed the data analysis together with the co-authors. I wrote the text.

6. Sammanfattning på svenska

(Warning! This chapter is not recommended for the opponent, or any other non-Swedish speaking reader, of this PhD thesis. Reading Swedish without knowing the language might cause confusion and headache.)

Den här avhandlingen fokuserar på den yttre delen av planeten Saturnus praktfulla ringsystem. Resultaten baseras på data från Cassini satelliten, som är i omloppsbana runt Saturnus sen 2004. I huvudsak har vi använt oss av data från Cassinis Langmuirprob, som är en ledande sensor gjord av titan och titannitrid. Langmuirproben gör in situ mätningar av de laddade partiklar, d.v.s. plasmat, som befinner sig runt Saturnus. När proben ges en negativ/positiv spänning så attraheras joner/elektroner så att en ström genereras. Storleken på strömmen beror på plasmats egenskaper, så från strömmen kan vi uppskatta plasmats densitet, hastighet och temperatur.

Större delen av vårt solsystem (och det observerbara universum) består av plasma, d.v.s. fria elektroner och joner. Vår sol består av plasma som i små mängder, jämfört med solens massa, hela tiden strömmar ut i och fyller upp vårt solsystem. Denna ström av partiklar kallas solvinden. När solvinden stöter på en planets magnetfält så böjs partikelns bana av och ett särskilt område i rymden runt planeten skapas, detta område kallas planetens magnetosfär.

En av Cassinis viktigaste upptäckter är att Saturnus måne Enceladus har stora sprickor i sitt isskal varifrån vatten och vattenånga konstant sprutar ut från det hav som döljer sig under isytan. Dessa plymer av vatten är också vad som anses vara den största källan till det material av vattenmolekyler och isstoft som finns i den inre delen av Saturnus magnetosfär. När dessa molekyler joniseras av elektronkollisioner eller av solens strålning så skapas plasma. I den här avhandlingen presenterar vi resultat från flera år av Langmuirprobsmätningar av plasmat i Saturnus inre magnetosfär. I Artikel I använder vi 5 års mätningar för att visa plasmadiskens utbredning. Våra resultat visar att plasmadiskdensiteter över $\sim$20 joner/cm^3 återfinns mellan 2.7 och 8.8 Saturnus radier R_S (där 1 R_S = 60 268 km) med en utsträckning i z-riktningen (d.v.s norr-söder) av ± 1 R_S. När vi begränsar vår studie till densitetsmätningar i ekvatorialplanet så visar det ett densitetsmaximum vid Enceladus bana, som motsvarar genomflygningar av Enceladusplymen. Dessa mätningar visar densiteter på 10^5 joner/cm^3. Utanför plymen är densiteterna mycket lägre, i stort sett aldrig över 150 joner/m^3. En viktig upptäckt är att densiteterna varierar mycket mer än vad som var förväntat. För, till exempel, avståndet 5 R_S från Saturnus mittpunkt, så varierar densiteterna mellan 20 och 110 joner/m^3. Detta

beror troligtvis på att plasmadisken är väldigt dynamisk, vilket vi undersökte i Artikel II.

I Artikel II visar vi att Saturnus inre plasmadisk har en stark dag/natt-asymmetri. Vi visar att jonhastigheterna i området 4 till 6 R_S varierar med 5-12 km/s, för ett valt radiellt avstånd, mellan dagsidan av Saturnus och nattsidan. Hastigheterna är högre på nattsidan. Detta ger upphov till att partiklarna som kretsar runt Saturnus får banor som är skiftade i riktning mot solen. Det visar sig också i dom uppmätta densiteterna som är högre på nattsidan än på dagsidan, för samma radiella avstånd. Densiteterna i området 4 till 6 R_S är nästan dubbelt så stora på nattsidan. Vi föreslå att det kan bero på en interaktion mellan laddat stoft och joner i plasmadisken. Stoftkornen, som är mycket större än jonerna, påverkas mer av strålningstrycket från solen. Strålningstrycket i samverkan med Saturnus magnetfält ger upphov till en extra jondrift som kan vara den vi uppmäter.

I Artikel III undersöker vi de kemiska reaktionerna som pågår i plasmadisken. Vi beräknar hur många joner per sekund som försvinner på grund av rekombination och jämför det med hur mycket som försvinner på grund av det radiella utflödet. Vår undersökning visar att förlusten på grund av transport dominerar förlusten på grund av rekombination i hela plasmadisken. Vi visar också att kemisk förlust ändå kan vara viktigt för plasmadiskens struktur i Enceladus närområde, där skillnaden i förlusterna bara är omkring en faktor 2.

I Artikel IV så använder vi ett större dataset, 8 år av mätningar, för att bland annat visa att dag/natt-asymmetrin även kan detekteras för denna tidsperiod. Vi bekräftar även mätningar som visar att den inre delen av plasmadisken varierar med tiden.

Genom vår forskning så har vi kunnat bidra med förståelse för hur Saturnus närområde ser ut och fungerar. En förståelse som är värdefull inte bara för att vi ska förstå Saturnus, men som också är nödvändig när man planerar nya missioner, både till Saturnus och till andra gasjättar med liknande plasmaförhållanden.

References

Ågren, K., Edberg, N. J. T., Wahlund, J.-E., 2012. Detection of negative ions in the deep ionosphere of Titan during the Cassini T70 flyby. Geophysical Research Letters 39, 10201.

Achilleos, N., Arridge, C. S., Bertucci, C., Jackman, C. M., Dougherty, M. K., Khurana, K. K., Russell, C. T., 2008. Large-scale dynamics of Saturn's magnetopause: Observations by Cassini. Journal of Geophysical Research: Space Physics 113 (A11), A11209.

Andriopoulou, M., Roussos, E., Krupp, N., Paranicas, C., Thomsen, M., Krimigis, S., Dougherty, M., Glassmeier, K.-H., 2012. A noon-to-midnight electric field and nightside dynamics in Saturn's inner magnetosphere, using microsignature observations. Icarus 220 (2), 503 – 513.

Andriopoulou, M., Roussos, E., Krupp, N., Paranicas, C., Thomsen, M., Krimigis, S., Dougherty, M., Glassmeier, K.-H., 2014. Spatial and temporal dependence of the convective electric field in Saturn's inner magnetosphere. Icarus 229, 57 – 70.

Arridge, C. S., Russell, C. T., Khurana, K. K., Achilleos, N., Cowley, S. W. H., Dougherty, M. K., Southwood, D. J., Bunce, E. J., 2008. Saturn's magnetodisc current sheet. Journal of Geophysical Research: Space Physics 113 (A4), A04214.

Bertucci, C., Hamilton, D. C., Kurth, W. S., Hospodarsky, G., Mitchell, D., Sergis, N., Edberg, N. J. T., Dougherty, M. K., 2015. Titan's interaction with the supersonic solar wind. Geophysical Research Letters 42 (2), 193–200.

Brace, L. H., Hoegy, W. R., Theis, R. F., 1988. Solar EUV measurements at Venus based on photoelectron emission from the Pioneer Venus Langmuir probe. Journal of Geophysical Research 93, 7282–7296.

Cassidy, T. A., Johnson, R. E., 2010. Collisional spreading of Enceladus' neutral torus. Icarus 209, 696–703.

Cowley, S. W. H., Bunce, E. J., 2003. Corotation-driven magnetosphere-ionosphere coupling currents in saturn's magnetosphere and their relation to the auroras. Annales Geophysicae 21, 1691 – 1707.

Dougherty, M. K., Khurana, K. K., Neubauer, F. M., Russell, C. T., Saur, J., Leisner, J. S., Burton, M. E., 2006. Identification of a Dynamic Atmosphere at Enceladus with the Cassini Magnetometer. Science 311 (5766), 1406–1409.

Fahleson, U., 1967. Theory of electric field measurements conducted in the magnetosphere with electric probes. Space Science Reviews 7, 238–262.

Fleshman, B. L., Delamere, P. A., Bagenal, F., 2010. A sensitivity study of the Enceladus torus. Journal of Geophysical Research: Planets 115 (E4), E04007.

Fleshman, B. L., Delamere, P. A., Bagenal, F., Cassidy, T., 2013. A 1-D model of physical chemistry in Saturn's inner magnetosphere. Journal of Geophysical Research (Planets) 118, 1567–1581.

Grard, R. J. L., 1973. Properties of the satellite photoelectron sheath derived from photoemission laboratory measurements. Journal of Geophysical Research 78 (16), 2885–2906.

Gurnett, D. A., Kurth, W. S., Kirchner, D. L., Hospodarsky, G. B., Averkamp, T. F., Zarka, P., Lecacheux, A., Manning, R., Roux, A., Canu, P., Cornilleau-Wehrlin, N., Galopeau, P., Meyer, A., Boström, R., Gustafsson, G., Wahlund, J.-E., Åhlén, L., Rucker, H. O., Ladreiter, H. P., Macher, W., Woolliscroft, L. J. C., Alleyne, H., Kaiser, M. L., Desch, M. D., Farrell, W. M., Harvey, C. C., Louarn, P., Kellogg, P. J., Goetz, K., Pedersen, A., 2004. The Cassini radio and plasma wave investigation. Space Science Reviews 114, 395–463.

Gurnett, D. A., Persoon, A. M., Kurth, W. S., Groene, J. B., Averkamp, T. F., Dougherty, M. K., Southwood, D. J., 2007. The variable rotation period of the inner region of Saturn's plasma disk. Science 316 (5823), 442–445.

Gustafsson, G., Wahlund, J., 2010. Electron temperatures in Saturn's plasma disc. Planetary and Space Science 58, 1018–1025.

Hedman, M., Gosmeyer, C., Nicholson, P., Sotin, C., Brown, R., Clark, R., Baines, K., Buratti, B., Showalter, M., 2013. An observed correlation between plume activity and tidal stresses on Enceladus. Nature 500, 182–184.

Helled, R., Galanti, E., Kaspi, Y., 2015. Saturn's fast spin determined from its gravitational field and oblateness. Nature 520, 2010–204.

Hill, T., 1979. Inertial limit on corotation. Journal of Geophysical Research: Space Physics 84 (A11), 6554–6558.

Hill, T. W., Thomsen, M. F., Tokar, R. L., Coates, A. J., Lewis, G. R., Young, D. T., Crary, F. J., Baragiola, R. A., Johnson, R. E., Dong, Y., Wilson, R. J., Jones, G. H., Wahlund, J.-E., Mitchell, D. G., Horányi, M., 2012. Charged nanograins in the Enceladus plume. Journal of Geophysical Research: Space Physics 117 (A5), A05209.

Høymork, S. H. (Ed.), 2000. Sensors and Instruments for Space Exploration, 2nd Edition. Swedish Institute of Space Physics, Kiruna, Ch. 7. Langmuir probes, pp. 121–145.

Jones, G. H., Arridge, C. S., Coates, A. J., Lewis, G. R., Kanani, S., Wellbrock, A., Young, D. T., Crary, F. J., Tokar, R. L., Wilson, R. J., Hill, T. W., Johnson, R. E., Mitchell, D. G., Schmidt, J., Kempf, S., Beckmann, U., Russell, C. T., Jia, Y. D., Dougherty, M. K., Waite, J. H., Magee, B. A., 2009. Fine jet structure of electrically charged grains in Enceladus' plume. Geophysical Research Letters 36 (16), L16204.

Kanani, S. J., Arridge, C. S., Jones, G. H., Fazakerley, A. N., McAndrews, H. J., Sergis, N., Krimigis, S. M., Dougherty, M. K., Coates, A. J., Young, D. T., Hansen, K. C., Krupp, N., 2010. A new form of Saturn's magnetopause using a dynamic pressure balance model, based on in situ, multi-instrument Cassini measurements. Journal of Geophysical Research: Space Physics 115 (A6), A06207.

Krimigis, S., Mitchell, D., Hamilton, D., Livi, S., Dandouras, J., Jaskulek, S., Armstrong, T., Boldt, J., Cheng, A., Gloeckler, G., Hayes, J., Hsieh, K., Ip, W.-H., Keath, E., Kirsch, E., Krupp, N., Lanzerotti, L., Lundgren, R., Mauk, B., McEntire, R., Roelof, E., Schlemm, C., Tossman, B., Wilken, B., Williams, D., 2004. Magnetosphere IMaging Instrument (MIMI) on the Cassini mission to Saturn/Titan. Space Science Reviews 114 (1-4), 233–329.

Laframboise, J. G., Parker, L. W., 1973. Probe design for orbit-limited current collection. The Physics of Fluids 16, 629–636.

Masters, A., Achilleos, N., Dougherty, M. K., Slavin, J. A., Hospodarsky, G. B., Arridge, C. S., Coates, A. J., 2008. An empirical model of Saturn's bow shock: Cassini observations of shock location and shape. Journal of Geophysical Research: Space Physics 113 (A10), A10210.

Morooka, M. W., Wahlund, J.-E., Eriksson, A. I., Farrell, W. M., Gurnett, D. A., Kurth, W. S., Persoon, A. M., Shafiq, M., André, M., Holmberg, M. K. G., 2011. Dusty plasma in the vicinity of Enceladus. Journal of Geophysical Research 116, A12221.

Mott-Smith, H. M., Langmuir, I., 1926. The theory of collectors in gaseous discharges. Physical Review 28, 727–763.

Ness, N. F., Acuna, M. H., Behannon, K. W., Neubauer, F. M., 1982. The induced magnetosphere of Titan. Journal of Geophysical Research: Space Physics 87 (A3), 1369–1381.

Persoon, A. M., Gurnett, D. A., Kurth, W. S., Groene, J. B., Faden, J. B., 2015. Evidence for a seasonally dependent ring plasma in the region between Saturn's A Ring and Enceladus' orbit. Journal of Geophysical Research: Space Physics 120 (8), 6276–6285.

Persoon, A. M., Gurnett, D. A., Kurth, W. S., Hospodarsky, G. B., Groene, J. B., Canu, P., Dougherty, M. K., 2005. Equatorial electron density measurements in Saturn's inner magnetosphere. Geophysical Research Letters 32, L23105.

Persoon, A. M., Gurnett, D. A., Leisner, J. S., Kurth, W. S., Groene, J. B., Faden, J. B., 2013. The plasma density distribution in the inner region of Saturn's magnetosphere. Journal of Geophysical Research: Space Physics 118 (6), 2970–2974.

Persoon, A. M., Gurnett, D. A., Santolik, O., Kurth, W. S., Faden, J. B., Groene, J. B., Lewis, G. R., Coates, A. J., Wilson, R. J., Tokar, R. L., Wahlund, J.-E., Moncuquet, M., 2009. A diffusive equilibrium model for the plasma density in Saturn's magnetosphere. Journal of Geophysical Research 114, 4211–4229.

Richardson, J. D., 1986. Thermal ions at Saturn: Plasma parameters and implications. Journal of Geophysical Research: Space Physics 91 (A2), 1381–1389.

Rymer, A. M., Mauk, B. H., Hill, T. W., Paranicas, C., André, N., Sittler, E. C., Mitchell, D. G., Smith, H. T., Johnson, R. E., Coates, A. J., Young, D. T., Bolton, S. J., Thomsen, M. F., Dougherty, M. K., 2007. Electron sources in Saturn's magnetosphere. Journal of Geophysical Research (Space Physics) 112, A02201.

Saur, J., Mauk, B. H., Kaßner, A., Neubauer, F. M., 2004. A model for the azimuthal plasma velocity in Saturn's magnetosphere. Journal of Geophysical Research: Space Physics 109 (A5), A05217.

Schippers, P., Moncuquet, M., Meyer-Vernet, N., Lecacheux, A., 2013. Core electron temperature and density in the innermost Saturn's magnetosphere from HF power spectra analysis on Cassini. Journal of Geophysical Research Space Physics 118, 7170–7180.

Sittler, E., Thomsen, M., Johnson, R., Hartle, R., Burger, M., Chornay, D., Shappirio, M., Simpson, D., Smith, H., Coates, A., Rymer, A., McComas, D., Young, D., Reisenfeld, D., Dougherty, M., André, N., 2006. Cassini observations of Saturn's inner plasmasphere: Saturn Orbit Insertion results. Planetary and Space Science 54 (12), 1197 – 1210.

Sittler, E. C., Andre, N., Blanc, M., Burger, M., Johnson, R. E., Coates, A., Rymer, A., Reisenfeld, D., Thomsen, M. F., Persoon, A., Dougherty, M., Smith, H. T., Baragiola, R. A., Hartle, R. E., Chornay, D., Shappirio, M. D., Simpson, D., McComas, D. J., Young, D. T., Jan. 2008. Ion and neutral sources and sinks within Saturn's inner magnetosphere: Cassini results. Planetary and Space Science 56, 3–18.

Thomsen, M. F., Reisenfeld, D. B., Delapp, D. M., Tokar, R. L., Young, D. T., Crary, F. J., Sittler, E. C., McGraw, M. A., Williams, J. D., 2010. Survey of ion plasma parameters in Saturn's magnetosphere. Journal of Geophysical Research 115 (A10), 1–22.

Thomsen, M. F., Roussos, E., Andriopoulou, M., Kollmann, P., Arridge, C. S., Paranicas, C. P., Gurnett, D. A., Powell, R. L., Tokar, R. L., Young, D. T., 2012. Saturn's inner magnetospheric convection pattern: Further evidence. Journal of Geophysical Research: Space Physics 117 (A9), A09208.

Wahlund, J.-E., Boström, R., Gustafsson, G., Gurnett, D. A., Kurth, W. S., Averkamp, T., Hospodarsky, G. B., Persoon, A. M., Canu, P., Pedersen, A., Desch, M. D., Eriksson, A. I., Gill, R., Morooka, M. W., André, M., 2005. The inner magnetosphere of Saturn: Cassini RPWS cold plasma results from the first encounter. Geophysical Research Letters 32 (20), L20S09.

Wilson, R., Bagenal, F., Delamere, P., Desroche, M., Fleshman, B., Dols, V., 2013. Evidence from radial velocity measurements of a global electric field in Saturn's inner magnetosphere. Journal of Geophysical Research 118, 1–11.

Wilson, R. J., Tokar, R. L., Henderson, M. G., 2009. Thermal ion flow in Saturn's inner magnetosphere measured by the Cassini plasma spectrometer: A signature of the Enceladus torus? Geophysical Research Letters 36 (23), L23104.

Wilson, R. J., Tokar, R. L., Henderson, M. G., Hill, T. W., Thomsen, M. F., Pontius Jr., D. H., 2008. Cassini plasma spectrometer thermal ion measurements in Saturn's inner magnetosphere. Journal of Geophysical Research 113, A12218.

Young, D. T., Berthelier, J.-J., Blanc, M., Burch, J. L., Bolton, S., Coates, A. J., Crary, F. J., Goldstein, R., Grande, M., Hill, T. W., Johnson, R. E., Baragiola, R. A., Kelha, V., McComas, D. J., Mursula, K., Sittler, E. C., Svenes, K. R., Szegö, K., Tanskanen, P., Thomsen, M. F., Bakshi, S., Barraclough, B. L., Bebesi, Z., Delapp, D., Dunlop, M. W., Gosling, J. T., Furman, J. D., Gilbert, L. K., Glenn, D., Holmlund, C., Illiano, J.-M., Lewis, G. R., Linder, D. R., Maurice, S., McAndrews, H. J., Narheim, B. T., Pallier, E., Reisenfeld, D., Rymer, A. M., Smith, H. T., Tokar, R. L., Vilppola, J., Zinsmeyer, C., 2005. Composition and Dynamics of Plasma in Saturn's Magnetosphere. Science 307 (5713), 1262–1266.

Acta Universitatis Upsaliensis

Digital Comprehensive Summaries of Uppsala Dissertations from the Faculty of Science and Technology 1298

Editor: The Dean of the Faculty of Science and Technology

A doctoral dissertation from the Faculty of Science and Technology, Uppsala University, is usually a summary of a number of papers. A few copies of the complete dissertation are kept at major Swedish research libraries, while the summary alone is distributed internationally through the series Digital Comprehensive Summaries of Uppsala Dissertations from the Faculty of Science and Technology. (Prior to January, 2005, the series was published under the title "Comprehensive Summaries of Uppsala Dissertations from the Faculty of Science and Technology".)

Distribution: publications.uu.se
urn:nbn:se:uu:diva-263278

ACTA
UNIVERSITATIS
UPSALIENSIS
UPPSALA
2015